

1 Antibiotics select for novel pathways of resistance in biofilms

2

3

4 Eleftheria Trampari¹, Emma R Holden¹, Gregory J Wickham¹, Anuradha Ravi¹,

5 Filippo Prischi³, Leonardo de Oliveira Martins¹, George M Savva¹, Vassiliy N. Bavro³,

6 Mark A Webber^{1,2*}

7

8

9 ¹Quadram Institute Bioscience, Norwich Research Park, Norwich, Norfolk, NR4 7UQ,

10 U.K.

11 ²Medical School, University of East Anglia, Norwich Research Park, Norwich,

12 Norfolk, NR4 7UA, U.K.

13 ³School of Biological Sciences, University of Essex, Wivenhoe Park, Colchester,

14 CO4 3SQ, U.K.

15

16

17 *mark.webber@quadram.ac.uk +

18

19 Keywords: evolution, efflux, multidrug resistance, *Salmonella*, AcrB

20 **Abstract**

21 Most bacteria in nature exist in aggregated communities known as biofilms. Bacteria
22 within biofilms are inherently highly resistant to antibiotics. Current understanding of
23 the evolution and mechanisms of antibiotic resistance is largely derived from work
24 from cells in liquid culture and it is unclear whether biofilms adapt and evolve in
25 response to sub-inhibitory concentrations of drugs. Here we used a biofilm evolution
26 model to show that biofilms of a model food borne pathogen, *Salmonella*
27 Typhimurium rapidly evolve in response to exposure to three clinically important
28 antibiotics. Whilst the model strongly selected for improved biofilm formation in the
29 absence of any drug, once antibiotics were introduced the need to adapt to the drug
30 was more important than the selection for improved biofilm formation. Adaptation to
31 antibiotic stress imposed a marked cost in biofilm formation, particularly evident for
32 populations exposed to cefotaxime and azithromycin. We identified distinct
33 resistance phenotypes in biofilms compared to corresponding planktonic control
34 cultures and characterised new mechanisms of resistance to cefotaxime and
35 azithromycin. Novel substitutions within the multidrug efflux transporter, AcrB were
36 identified and validated as impacting drug export as well as changes in regulators of
37 this efflux system. There were clear fitness costs identified and associated with
38 different evolutionary trajectories. Our results demonstrate that biofilms adapt rapidly
39 to low concentrations of antibiotics and the mechanisms of adaptation are novel.
40 This work will be a starting point for studies to further examine biofilm specific
41 pathways of adaptation which inform future antibiotic use.

42

43 **Main**

44 Antimicrobial resistance (AMR) is a complex problem and is a major threat to human
45 and animal health (1). Understanding how bacteria develop resistance to antibiotics
46 is important to inform how they should be used to minimise selection of AMR. There
47 are many genetic mechanisms of antibiotic resistance and the selection of resistant
48 mutants is a classic example of natural selection (2). Initial studies of mechanisms of
49 resistance tended to expose populations to very high concentrations of antibiotics
50 and select for survivors. This identified 'high-impact' mutations can confer a large
51 phenotypic benefit and proved very useful for characterising cellular targets and
52 primary resistance mechanisms. However, more recent work has found that
53 repeated exposure to sub-inhibitory concentrations of antimicrobials can have
54 profound impacts on bacterial populations including selection for high level
55 resistance (3,4). This better reflects real world situations where low levels of
56 antimicrobials are commonly present. Importantly, this allows epistatic interactions
57 between multiple genes to be selected and for fitness costs arising from resistance
58 mutations to be ameliorated by additional, compensatory mutations (5).

59 Much of our understanding of the mechanisms of antibiotic action and resistance
60 comes from laboratory experiments in which bacteria are routinely grown in liquid
61 culture before being exposed to antibiotics. Yet most bacteria in nature exist in
62 biofilms; aggregates of cells often attached to a surface (6). Biofilms represent a
63 fundamentally different mode of life to planktonic cultures and multiple studies have
64 demonstrated extreme changes in gene and protein expression profiles from the
65 same strains when grown in liquid or as a biofilm (7). Many infections include a
66 biofilm component which makes the infection difficult to treat; common examples
67 include infections on prosthetic or indwelling devices. One of the hallmarks of

68 biofilms is inherit resistance to antibiotics, when compared to the corresponding
69 strain grown in liquid culture. One theory explaining the high degree of resistance to
70 antibiotics in biofilms is that cells within a biofilm are metabolically inactive, or even
71 'persisters'. In these dormant subpopulations, characterised by arrested
72 macromolecular syntheses, the cellular targets which the antibiotics poison are not
73 essential, thus impeding the bactericidal activity of the antibiotic (8). However, recent
74 studies have demonstrated a strong evolutionary pressure for strains to evolve
75 improved biofilms. In particular, rapid selection of mutants and combinations of
76 mutants with improved biofilm fitness is observed when bacteria are introduced to a
77 new niche (9–11).

78 Given this evidence of adaptation within biofilms we were interested whether
79 exposure to low concentrations of antibiotics would exert a selective effect on cells
80 within a biofilm. We hypothesised that exposure of biofilms to sub-lethal
81 concentrations of antibiotics would impart a selective pressure and the outcomes of
82 this stress would be distinct to those seen in planktonic cells. To test this hypothesis,
83 we adapted an experimental biofilm evolution model and used *Salmonella*
84 Typhimurium as a model biofilm-forming pathogen which we exposed to three
85 clinically relevant antibiotics. We compared drug exposed biofilm lineages to
86 unexposed biofilm controls and exposed planktonic lineages. We measured the
87 emergence of antibiotic resistance, biofilm capacity, and pathogenicity, and
88 subsequently investigated condition-specific mechanisms of resistance using
89 genome sequencing. We observed rapid adaptation to antibiotic pressure which
90 often carried a cost for biofilm formation, identified novel mechanisms of resistance
91 against cefotaxime and azithromycin and detected biofilm-specific phenotypes

92 showing that studying how biofilms adapt to stress is vital to understanding the
93 evolution of AMR.

94 **Results**

95 **A biofilm evolution model can study responses to antimicrobial stress**

96 To study the evolution and adaptation of *S. Typhimurium* biofilms when exposed to
97 antibiotics, a serial transfer bead-based model system was adapted and optimised
98 (based on previous work by the Cooper group (11)). To establish *Salmonella*
99 biofilms, we grew bacteria on glass beads in broth (see materials and methods). The
100 beads served as a substrate for biofilms to form on and as a biofilm transfer vehicle,
101 used to move mature biofilms to new tubes with fresh media and new sterile beads.
102 After each transfer, bacteria from the biofilm community had to colonise the new
103 beads and establish biofilms on their surface before being transferred again. This
104 system allows repeated longitudinal exposure of biofilms to the stress of interest and
105 captures all the major components of the biofilm lifecycle. After each passage, cells
106 from biofilms were harvested and populations and individual representative strains
107 were stored and phenotypically characterised. Strains that developed resistance or
108 exhibited altered biofilm formation were selected for whole-genome-sequencing to
109 identify the genetic basis of these phenotypes (Figure 1, a-d).

110 To determine the appropriate conditions for the evolution experiments, we measured
111 biofilm formation by *S. Typhimurium* 14028S in lysogeny broth (without salt) after 24,
112 48, 72 and 96 hours, at 25°C, 30°C, 37°C and 40°C respectively (Figure 1, e). Biofilm
113 formation was determined by measuring cfu per bead (Figure 1, e). Over 72 hours
114 the highest amount of biomass formed ($\sim 10^6$ cfu/ bead) was after incubation at 25°C

115 or 30°C; this was stable and consistent. Therefore, we ran the evolution experiments
116 at 30°C with a passage period of 72 hours.

117 To investigate if and how biofilms would adapt to exposure to sub-inhibitory
118 concentrations of antibiotics, we grew biofilms on beads, in the presence of three
119 clinically-important antibiotics for the treatment of Salmonellosis; azithromycin,
120 cefotaxime and ciprofloxacin. The minimum inhibitory concentrations (MICs) for each
121 antibiotic were determined following the EUCAST microbroth dilution method,
122 adapted to use LB-NaCl and 30 °C to replicate the experimental conditions. Growth
123 kinetics in the presence of all three agents were determined at the same conditions.
124 Based on these results we identified concentrations of each agent (10 µg/mL
125 azithromycin, 0.062 µg/mL cefotaxime and 0.015 µg/mL of ciprofloxacin) that reliably
126 restricted planktonic growth rates to approximately 50% of that of unstressed control
127 cultures which were then used for evolution experiments. This approach had proved
128 tractable in our previous planktonic evolution experiments with biocides (12).

129 We ran three separate evolution experiments, one with each antibiotic. Within each
130 we included eight lineages; four exposed bead lineages, two exposed planktonic
131 cultures and two drug-free bead-control lineages (Figure 1b). Populations from early,
132 middle and late time points of each experiment were harvested from beads and three
133 single colonies were isolated to allow us to examine phenotypic diversity within the
134 population. The isolates were tested for their biofilm ability, morphology and
135 susceptibility. Biofilm formation was monitored using the Crystal Violet assay (CV)
136 assay and matrix production assessed qualitatively by visualising colonies grown on
137 Congo Red (CR) plates. Susceptibility to antibiotics was measured by determining
138 MICs using the agar dilution method (13).

139 To confirm the model selects for evolution of increased biofilm formation we
140 phenotyped isolated single cells from drug-free bead-control lineages. We observed
141 an incremental increase in biofilm formation with unexposed isolated colonies
142 forming larger and wrinklier biofilms on CR plates and producing more than three
143 times as much biomass over the course of the experiment (Figure 1, f). This
144 confirmed the model strongly selects for adaptation to produce biofilms with
145 increased biomass over time in the absence of any stressor.

146 **Biofilms rapidly evolve and adapt in response to sub-inhibitory antibiotic** 147 **concentrations**

148 To test the phenotypic responses of biofilms repeatedly exposed to non-lethal
149 concentrations of the test antibiotics, we isolated both populations and three
150 individual strains from each lineage at three different timepoints of all experiments;
151 early (first passage), mid (half way point) and late (final passage). We characterised
152 these populations as well as isolated strains for susceptibility to eight clinically-
153 relevant antimicrobials, biofilm formation and colony morphology. We compared
154 results from the biofilm lineages with the corresponding planktonic lineages run at
155 the same time (Figure 2).

156 Biofilms rapidly evolved resistance in response to all three exposures (Figure 2). The
157 time taken to select for emergence of mutants with decreased susceptibility to the
158 antibiotics was similar in both biofilm and planktonic lineages. Azithromycin selected
159 mutants in a stepwise manner with emergence of a population with an 8-fold MIC
160 increase, followed by selection of highly resistant populations with MICs of
161 azithromycin 16 times more than the parent strain. The decreased susceptibility of
162 the azithromycin-exposed lineages became evident at the earliest time point and
163 was fixed by the mid-point of the experiment (Figure 2 a, b). Cefotaxime

164 demonstrated a similar dynamic with both planktonic populations and biofilms
165 exhibiting decreased susceptibility and maintaining this resistance profile until the
166 end of the experiment (Figure 2, c-d). Adaptation to ciprofloxacin resistance was
167 selected by the middle of the experimental period and remained fixed up to the final
168 timepoint in both biofilm and planktonic lineages (Figure 2 e, f).

169 While the selection dynamics seemed similar between biofilm and planktonic
170 lineages at first glance, analysis of the MICs to all the antibiotics tested, revealed
171 significant differences in the outcomes between biofilm and planktonic conditions.
172 For instance, whilst planktonic populations, exposed to cefotaxime, become mainly
173 resistant to cefotaxime, cefotaxime-exposed biofilms exhibited a multidrug resistance
174 (MDR) phenotype (Figure 2, d). These observations show that whilst the biofilms are
175 able to develop resistance to the selective antibiotics, the mechanisms are likely to
176 be distinct to those seen in planktonic culture.

177 Whilst it is widely accepted that increased biomass and matrix production improves
178 resilience of biofilms to antimicrobial stress, we observed that biofilm formation itself
179 is heavily influenced by the selective antibiotic. For example, azithromycin prevented
180 the strains from adapting and forming better biofilms whereas unexposed biofilms
181 produced much more biomass over time (Figure 2b). Cefotaxime had a strong
182 negative effect on biofilm formation, with biofilms exposed to cefotaxime actually
183 producing less biomass than the starting wild-type strain and being characterised by
184 pale colony morphology on CR plates (Figure 2d). Ciprofloxacin had less impact on
185 biofilm formation and biofilms exposed to this drug produced increased biomass over
186 time, although to only half the level of the control biofilms. As expected, isolates from
187 planktonic lineages did not form better biofilms over time. On the contrary,

188 cefotaxime exposure again selected for weaker biofilms with a pale colony
189 morphology on CR plates (Figure 2c).

190 **Individual antibiotics select specific pathways to resistance in biofilms**

191 To investigate correlations between development of resistance to different antibiotics
192 and biofilm formation after each exposure, we compared fold changes in MIC of
193 antibiotics with fold changes in biofilm formation (Figure 3). Each point on the graphs
194 represents a single isolated strain from each evolution experiment (blue:
195 azithromycin exposure, white: cefotaxime exposure, red: cipro exposure, black: drug
196 free exposed controls). All results were compared to averaged data from the parent
197 strain (represented as point '0,0' on the graphs).

198 As expected, strains became resistant to the antibiotic they were exposed to. There
199 were also examples of selection of cross-resistance to other antibiotics in the
200 biofilms. For instance, azithromycin-exposed isolates exhibited an MDR phenotype
201 and demonstrated decreased susceptibility not only to azithromycin, but also to
202 cefotaxime, chloramphenicol, ciprofloxacin, nalidixic acid, tetracycline and triclosan.
203 Similarly, the cefotaxime-exposed lineages showed increased MICs of
204 chloramphenicol and tetracycline. Most of the antimicrobials tested are known
205 substrates of multidrug efflux pumps (e.g. AcrAB-TolC) except for kanamycin.
206 Strikingly, this was the only antibiotic to which no cross-resistance was observed. In
207 fact, cefotaxime exposed isolates became more susceptible to kanamycin than the
208 parent strains.

209 Apart from impacts on antibiotic resistance, antibiotic exposure also resulted in major
210 changes in the strains' ability to form biofilms. Bacteria exposed to cefotaxime
211 exhibited severely compromised biofilm ability, whereas azithromycin and

212 ciprofloxacin led to inhibition or delayed biofilm adaptation respectively. This analysis
213 again indicates that exposure to antibiotics prompts selection for resistance even at
214 sub-inhibitory concentrations, but that this comes at a cost to the ability to form
215 biofilms.

216 To identify the mechanisms responsible for the phenotypes described above, we
217 whole-genome sequenced over 100 strains (selected to represent major phenotypes
218 of interest and to cover different times in the exposure series for each drug) and
219 identified changes against the parent strain genome. We sequenced a mixture of
220 populations and single cells and used data from single-cell strains to analyse the
221 phylogeny of the mutants (Figure 4a). The results indicated that the different
222 antibiotics selected for mutants which followed distinct paths of adaptation. There
223 was little commonality between the drug exposures showing that there is no
224 universal or generic mechanism of resistance selected for in biofilms. Biofilms
225 exposed to azithromycin and cefotaxime followed a reproducible and distinct
226 evolution pattern (Figure 4b, c), whereas in the ciprofloxacin exposure, bacteria
227 responded to the stress in a number of different ways (Figure 4d). For all drugs,
228 there was separation of biofilm (darker coloured dots) and planktonic lineages
229 (lighter coloured dots) apparent in the phylogeny, again demonstrating different
230 trajectories of selection.

231 **Azithromycin and cefotaxime select novel mechanisms of resistance based**
232 **upon exclusion of drug from target which in turn hinders biofilm formation**

233 We used the whole-genome sequencing data to identify mutations which may
234 account for potential mechanisms of resistance against the antibiotics of interest.
235 These include some known mechanisms of resistance (e.g. *gyrA* mutation renders
236 bacteria resistant to quinolones (14–16)), as well as Single Nucleotide
237 Polymorphisms (SNPs) that have never been linked to antimicrobial resistance
238 before. The sequence data gave us enough information to build solid hypotheses
239 about the genetic basis for novel mechanisms of resistance against cefotaxime and
240 azithromycin, which we then tested experimentally using a combination of assays
241 (Figure 5).

242 *Novel mechanisms of cefotaxime resistance*

243 We first observed that isolates that became resistant to cefotaxime had two unique
244 substitutions that they acquired at different timepoints during the evolution
245 experiment. The first substitution was in EnvZ (corresponding to arginine 397 to
246 histidine) and the second was in AcrB (glutamine 176 to lysine).
247 EnvZ is an osmolarity-sensor protein, attached to the inner membrane of the cell. It
248 functions both as a histidine kinase and a phosphatase, exerting its activity by
249 altering the phosphorylation levels of its cognate transcriptional regulator OmpR.
250 OmpR, amongst other functions, is responsible for differential regulation of the
251 expression of OmpC and OmpF, two principal outer-membrane porins (17,18), as
252 well as curli biosynthesis through the *csgD-csgBAC* operon (19). Mutants carrying
253 the substitution of R397H in EnvZ exhibited a 4-fold increase in the MIC of
254 cefotaxime (Figure 5a) of cefotaxime and produced pale colonies on CR plates. This

255 substitution was present in both planktonic cultures and in biofilms. It is well
256 established that β -lactams cross the outer membrane via porin channels and
257 particularly through OmpF (20–22). It is also well known that OmpR stimulates curli
258 biogenesis by promoting expression of CsgD, which in turn activates the curli operon
259 (23).

260 AcrB is a key component of the tripartite multidrug efflux pump AcrAB-TolC, and is
261 responsible for substrate recognition and energy transduction (24–26) during the
262 efflux process. Being a member of the *Resistance Nodulation cell Division* (RND)
263 family, AcrB shares a common structural organisation with other RND pumps, and
264 couples inward proton transport to antiport (efflux) of a wide range of xenobiotic
265 agents including antibiotics, thus contributing to the emergence of MDR bacteria.
266 The identified Q176K substitution in AcrB was found in strains already containing the
267 EnvZ substitution and led to an additional 4-fold increase in the MIC of cefotaxime
268 (Figure 5a). This substitution was only detected from planktonic cultures and had no
269 additional impact on biofilm formation over that of the EnvZ R397H mutant.

270 Based on the above, we hypothesised that the ‘first-step’ changes in MIC were due
271 to alterations in expression of *ompC* and *ompF* following mutation of *envZ*.
272 Subsequent substitution in AcrB, was responsible for altered coordination of
273 cefotaxime by AcrB (Q176 is in the distal drug binding pocket of AcrB) and
274 correspondingly lowered residence time of the antibiotic in the pocket, leading to
275 increased efflux of this substrate. Changes in curli expression (due to loss of EnvZ-
276 mediated activation of OmpR), would account for the compromised biofilm formation
277 phenotype we observed for these isolates.

278 We tested this hypothesis in a number of ways. First, we isolated RNA from 48-hour
279 biofilms, grown in LB agar plates with no salt, formed by strains carrying the
280 identified substitutions (cef-biofilm-M-D-S1 (EnvZ R397H) and cef-plank-L-S2 (EnvZ
281 R397H/ AcrB Q176H)), as well as the WT strain as a control. We performed qRT-
282 PCR to measure *ompC* and *ompF* expression, using *gyrB* expression as our
283 reference (Figure 5b). We observed a significant reduction in *ompF* expression in
284 both the mutants as well as an overexpression of *ompC* indicating that the balance
285 of porin expression had been altered as predicted (Figure 5b). To test whether the
286 decrease in *ompF* led to reduced drug accumulation in the cells, we used a resazurin
287 drug accumulation assay which confirmed that, both mutants show reduced
288 accumulation of drugs inside the cell (Figure 5d).

289 Additionally, we measured expression of the main curli subunits, *csgA* and *csgB*, and
290 found that expression in the mutants was completely lost (Figure 5c). This explains
291 the pale phenotype on CR and supports our hypothesis that loss of EnvZ function
292 confers protection against cefotaxime, but at a cost to biofilm formation.

293 We confirmed the specific phenotypic impacts of the two substitutions by creating
294 mutants of the parent strain lacking *acrB* or *envZ* and complementing these with
295 either wild-type or mutant alleles and determining the impacts on phenotypes (Figure
296 5a). Deletion of *envZ* and complementation with the WT allele did not lead to any
297 MIC changes for any of the antibiotics tested. However, complementation with the
298 mutant pEnvZ R397H allele led to a significant increase in MICs of cefotaxime,
299 chloramphenicol and tetracycline. Similarly, although complementation of the AcrB
300 deletion strain with AcrB or AcrB Q176K did not have an impact on resistance,
301 complementation of AcrB in a Δ AcrB/ Δ RamR background with the Q176K allele led
302 to decreased susceptibility to cefotaxime, chloramphenicol and tetracycline,

303 replicating the phenotype of strains derived from the evolution experiments. These
304 results confirm that the mutations identified are responsible for the resistance
305 phenotypes observed after exposure to cefotaxime.

306 Finally, we performed *in silico* modelling work to investigate the potential impact of
307 the Q176K substitution on AcrB structure and substrate binding (Figure 4e-f).
308 AutoDock VINA docking simulations were used, allowing for flexible side-chains.
309 Analysis of cefotaxime docking, as well as docking of the control antibiotics,
310 nitrocefin and cephalothin, to both the WT (Q176) and the mutant (Q176K), were
311 based on experimental crystallographic studies (supplementary figure S1, a-b). The
312 analysis focused on the distal binding pocket of chain B of AcrB from *E.coli*
313 (4DX5.pdb) (27) corresponding to the “bound” or “tight” protomer conformation. We
314 found that in both cases, Q176 and the mutant side chain, Q176K, participated in the
315 coordination of cephalosporin molecules. However, the coordination was markedly
316 different, between the WT and the mutant, and resulted in statistically significant
317 reduction in the free energy of binding (ΔG) (Supplementary table S1). This supports
318 the idea that the substitution might cause a reduction in the residence time for drugs
319 in the pocket and as a result, increased efflux and decreased susceptibility.

320 *Novel mechanisms of azithromycin resistance*

321 Lineages exposed to azithromycin developed an 8-fold increase in azithromycin MIC
322 (reaching the proposed epidemiological cut-off to define resistance in *Salmonella*
323 (28)) before adapting further to have an MIC 16x higher than the parent (Figure 5f).
324 When we sequenced the resistant strains, we identified two distinct amino acid
325 substitutions. In the first population, there was an arginine 717 substitution to leucine

326 in AcrB and the mutants with highest MICs also had a threonine 18 substitution to
327 proline in RamR.

328 Interestingly, this substitution in AcrB is distinct from that observed after cefotaxime
329 exposure, and in a different part of the protein. The distal binding pocket is predicted
330 to control access of substrates into the pump, as well as participating in the
331 coordination of high-molecular mass substrates, such as macrolides in the proximal
332 binding pocket (29,30). This indicates that changes in different parts of AcrB confer
333 resistance to different substrates.

334 RamR is the transcriptional repressor of *ramA*, which is a global transcriptional
335 activator that positively regulates the AcrAB-TolC pump production (31). The
336 inactivation of *ramR* results in over-expression of RamA, consequently increasing
337 pump expression and inducing an MDR phenotype (32). We observed that isolates
338 with this substitution also acquired cross-resistance to cefotaxime, chloramphenicol,
339 nalidixic acid, tetracycline and triclosan, all of which are AcrB substrates.

340 Our hypothesis was that the R717L substitution in AcrB would result in increased
341 efficiency of efflux of azithromycin and as a result, increased resistance. The
342 additional RamR substitution would then result in over-expression of this mutant
343 pump and explain the further increase in the MIC of azithromycin. To test this
344 hypothesis, we extracted RNA from 48-hour old biofilms and we measured
345 expression of *acrB* and *ramA* by q-RT-PCR, again using *gyrB* expression as our
346 reference (Figure 5g). For both targets there was up-regulation in the mutants
347 compared to the parent strain although expression levels of *acrB* in all cells were
348 low; AcrB is primarily produced in growing cells so low levels of *acrB* mRNA was not
349 unexpected. Intracellular drug accumulation was monitored as described above

350 using the resazurin method (Figure 5h). The R717L mutant alone did not show any
351 changes in accumulation compared to the WT, suggesting the substitution does not
352 impact export of this substrate. This supports the idea that this change improves
353 access for larger substrates to the pump (such as azithromycin, Mr:749), which relies
354 on the proximal drug binding vetting. However, this would not impact a small
355 molecule like resazurin (Mr:229), which has been suggested to directly access the
356 distal binding pocket, by bypassing the proximal pocket of the pump (30,33).
357 Consistent with this idea was the observation of markedly reduced resazurin
358 accumulation in the double mutant, where pump over-expression would be expected
359 to reduce accumulation of a wide range of substrates and confer the typical efflux-
360 based MDR phenotype observed.

361 To confirm the causative impact of these mutations, we used the same approach as
362 for the cefotaxime mutations where we re-introduced mutant and wild-type alleles of
363 *acrB* and *ramR* into mutants lacking these genes to observe the impact (Figure 5f).
364 AcrB R717L introduction to the Δ *acrB* background led to increased resistance only
365 against azithromycin, complementing perfectly the phenotype of the adapted and
366 evolved strain carrying the AcrB R717L mutation. RamR T18P introduction to the
367 Δ *ramR* background led to an additional increase in MICs of azithromycin,
368 chloramphenicol, nalidixic acid and tetracycline, confirming the hypothesis that
369 overexpression of the efflux pump leads to an MDR response. These results confirm
370 that these are the mutations responsible for the resistant phenotypes observed after
371 exposure to azithromycin.

372 To investigate the impact of the R717L substitution on the structure and function of
373 AcrB, we performed molecular docking of azithromycin and erythromycin
374 (supplementary Figure S2, a-b) in the proximal binding site. The proximal binding

375 pocket is split into two distinct, yet overlapping macrolide binding sites, A and B. Site
376 A is known to be responsible for rifampicin binding, whereas, site B has been
377 associated with erythromycin binding and is located deeper into the proximal pocket
378 (30).

379 We first docked azithromycin in site B of the proximal binding pocket, producing a
380 model structure, which closely matches the experimental structure of AcrB with
381 erythromycin (3AOC.pbd, chain C, supplementary figure S2, a-b)(30). Our analysis
382 indicated that R717 is located too far away to directly interact with the drug, making it
383 unlikely for the observed coordination in site B to contribute to the observed
384 phenotype. To investigate whether R717 participates in earlier stages of the
385 substrate recognition pathway, we performed docking of azithromycin to site A,
386 located in the front part of the proximal binding pocket (Figure 4g). This showed
387 plausible coordination with direct involvement of R717, and also indicated a clear
388 energetic advantage of the R717 WT over R717L. In fact, R717L led to a radically
389 different coordination of azithromycin (Figure 4h, supplementary table S1),
390 rationalising the observed MDR phenotype.

391 **Drug resistance in biofilms is stable once selected but costs to virulence and** 392 **biofilm formation can be ameliorated by stress free passage**

393 We showed that control biofilms that have not been exposed to drugs rapidly
394 adapted to form better biofilms during the experiment (Figure 1f). However, when
395 these strains were tested for drug susceptibility, no changes were observed over
396 time (Figure 6a). There was also no correlation between biofilm ability and
397 antimicrobial susceptibility in these populations which were not exposed to any drugs
398 (Figure 6b). This shows that making more biomass does not alone affect antibiotic
399 susceptibility.

400 While we initially investigated whether biofilms have inherently altered susceptibility
401 to antibiotics using conventional susceptibility testing, we also tested whether
402 biofilms were more tolerant of drugs in context. To test whether biofilm-adapted
403 strains have a viability advantage when treated with antibiotics, we grew biofilms on
404 beads for 72 hours at 30°C, and then washed them and exposed them to a range of
405 ciprofloxacin concentrations (Figure 6c). To determine the survival rate, we isolated
406 and counted surviving cells. Survival was normalised against biofilms formed from
407 each strain unexposed to drug. We tested: a planktonic isolate which had been
408 exposed to ciprofloxacin (Cip-plank-L-S1), a control biofilm-adapted isolate not
409 exposed to any drug (biofilm-control-L-S1) and an exposed, biofilm adapted isolate
410 from the ciprofloxacin evolution experiment (Cip-biofilm-L-B-S3). The control biofilms
411 made significantly more biomass than the drug exposed biofilms but demonstrated
412 only a mild increase in survival to the drug treatment compared to the WT strain.
413 Biofilms formed by the drug-exposed planktonic lineage (adapted and highly
414 resistant to ciprofloxacin but with equivalent biofilm formation ability to the parent)
415 had also a mild increase in survival compared to WT biofilms. Interestingly, only
416 bacteria from the biofilm lineage exposed to ciprofloxacin exhibited a significant
417 survival increase even though this strain was no more resistant (by MIC) than the
418 planktonic mutant and made significantly less biofilm than the drug free control. This
419 suggests that neither specific resistance to ciprofloxacin or the ability to make more
420 biomass are enough to improve survival within a biofilm alone. To confirm these
421 results, we grew biofilms on coverslips for 72 hours at 30°C, treated them with 3
422 µg/mL ciprofloxacin for 90 minutes and carried out live/dead staining to visually
423 characterise survival by fluorescence microscopy (Figure 6d). Our first observation
424 was that, as expected, the different strains formed biofilms of variable density.

425 Survival was only obvious in the denser biofilm regions, where cells produced more
426 biomass and significant numbers of surviving cells were only observed in the
427 ciprofloxacin-exposed biofilm lineage. Visualisation of this biofilm showed denser
428 clusters of cells than the WT or biofilm-adapted lineage biofilms. Whilst the overall
429 level of biomass was not as high as drug free adapted controls for this strain, the
430 results suggest that a combination of improved biofilm formation and stress
431 adaptation are essential for biofilm viability and survival.

432 To test whether drug adaptation influences pathogenicity, we selected isolates from
433 different exposures and tested their virulence in the *Galleria mellonella* infection
434 model (Figure 6e, bar chart). Larvae were injected with strains representing different
435 biofilm and resistance phenotypes. Un-injected larvae as well as PBS controls were
436 included as appropriate and the wild type strain (14028S) was used as a reference.
437 In parallel we measured biofilm formation for all cultures used to inoculate larvae
438 using both the CV (Figure 6e, overlaid line graph on the right axis) and the CR
439 assay. We observed that strains with increased biofilm ability were the least
440 infectious, whereas isolates with weaker biofilm phenotypes were most pathogenic.
441 For example, biofilm-control-L-S1, which is a drug free control, biofilm-adapted
442 strain, caused the least deaths with a 95% survival rate. In comparison, Cip-biofilm-
443 M-B-S2, which is a drug-resistant but low-biofilm-forming strain, killed 50% of the
444 larvae. Hence, adaptation to the drug exposure had no obvious advantage for
445 pathogenicity. Our data suggests a strong correlation between pathogenicity and
446 biofilm formation but no association with resistance.

447 To test the stability of the phenotypes obtained during the course of the evolution
448 experiments, we selected resistant strains to the previous antibiotic exposures with
449 low and high biofilm forming abilities (see materials and methods) and put them

450 through a 24-hour passage, accelerated biofilm evolution experiment (Figure 6, f-i).
451 This was run for 10 days with passages every 24 hours without any antibiotics
452 present, to test whether the resistance and biofilm patterns change over time without
453 any selection. From each population, we isolated single strains and phenotyped
454 them for their biofilm ability and their susceptibility against the same panel of
455 antibiotics we used previously (see materials and methods). We observed that
456 resistance remained stable for most antibiotics (Figure 6f), while the overall ability of
457 the tested strains to form biofilms improved significantly over time ($p < 0.04$, Figure
458 6g). We also looked individually at the strains with initially low biofilm ability and
459 decreased susceptibility (azi-biofilm-M-B-S2, cef-biofilm-L-A-S1) and we observed
460 that stability of resistance is highly dependent on the nature of the stress. The MIC of
461 azithromycin did not significantly change over time for the azithromycin resistant
462 strain (Figure 6h, orange line), whereas the initially cefotaxime resistant strain
463 exhibited significantly reduced susceptibility by the end of the accelerated
464 experiment (Figure 6i, purple line). In both cases, the biofilm formation of the strains
465 was recovered (Figure 6, h-i).

466

467 **Discussion**

468 To develop new antimicrobial strategies, it is important that we understand the
469 genetic mechanisms responsible for bacterial resistance in relevant contexts.

470 Although the evolution of antimicrobial resistance is often studied, previous work has
471 largely focused on planktonic cells and not bacterial biofilms. While it is commonly
472 accepted that biofilms are inherently highly drug resistant, surprisingly little work
473 explores how biofilms evolve in response to antimicrobial stress. One recent report
474 showed that *Acinetobacter* biofilms do adapt to sub-lethal exposure to ciprofloxacin
475 and that mechanisms of resistance were distinct to those seen in planktonic controls
476 (34). Here we address this question using *Salmonella* biofilms as a model system
477 with multiple drugs.

478 The intrinsic resistance of biofilms to antimicrobials has been attributed to both
479 unique structural characteristics of biofilms but also the wide range of growth states
480 of cells present within biofilms, including dormant or persister cells (35–39). We
481 investigated whether these already resistant communities evolve and adapt further
482 when exposed to sub-inhibitory drug stress. We found that biofilms are highly
483 sensitive to sub-inhibitory exposure to antibiotics, which rapidly selected for changes
484 in the populations. Different stresses selected distinct patterns of adaptation, some
485 of which were unique to the biofilm communities. There was no common response to
486 all three drugs tested, which strongly suggests that there is not a common or generic
487 mechanism for antimicrobial resistance seen in biofilms but instead adaptation highly
488 depends on the nature of the stress.

489 When cells were exposed to azithromycin or cefotaxime, both planktonic and biofilm
490 populations became resistant not only to the selective drug but also to several

491 different antibiotics, indicating mechanisms conferring MDR. Strikingly, both
492 azithromycin and cefotaxime selected for highly-resistant populations, but also with a
493 marked attenuation of biofilm formation. Lineages exposed to ciprofloxacin were able
494 to improve biofilm formation over time although this was delayed compared to control
495 biofilms. The ciprofloxacin results are consistent with a recent observation from
496 *Acinetobacter* biofilms, where biofilm formation was not compromised after exposure
497 to the drug (34). It is clear from our results that selection of resistance within a biofilm
498 can have a major impact on important phenotypes that impact on bacterial fitness
499 and survival in the real world.

500 To determine the mechanisms underlying susceptibility, we sequenced more than
501 100 strains covering the different exposures and time points and demonstrating a
502 range of distinct susceptibility and biofilm phenotypes. Azithromycin exposure
503 selected for the same mutations (changes in AcrB and RamR) in independent
504 lineages, and these emerged in a step-wise manner over the course of the evolution
505 experiment. Similarly, exposure to cefotaxime selected for mutants with altered AcrB
506 and EnvZ, with the same substitution within EnvZ observed in independent lineages.
507 The primary aim of this work was to identify mechanisms rather than the detailed
508 evolutionary dynamics of selection, however the presence of identical substitutions in
509 multiple lineages is strong evidence for the importance of these changes.

510 Ciprofloxacin exposure selected for a wider variety of mutations with much more
511 variation in phenotypes indicating multiple paths of evolution and resistance. The
512 difference between the drugs is likely to reflect the mechanisms of action and
513 resistance; there are multiple known chromosomal mechanisms of ciprofloxacin
514 resistance (including target site changes, porin loss, efflux) whereas high-level
515 resistance to cefotaxime and azithromycin is often a result of acquisition of specific

516 enzymes. In this closed system, acquisition of DNA is not possible, so cells are
517 constrained to mutation of the core genome to generate resistant mutants. This
518 hypothesis was supported by analysis of the mechanisms of resistance.

519 After analysing the sequencing results, we were able to identify novel mechanisms of
520 resistance against cefotaxime and azithromycin respectively, which we then
521 confirmed experimentally.

522 We showed that strains exposed to cefotaxime demonstrated a two-step selection of
523 resistance with an initial four-fold rise in cefotaxime MIC, followed by an eight-fold
524 increase. This was linked to an initial R397H substitution in the EnvZ protein followed
525 by an additional Q176K genetic substitution in AcrB. We showed that the EnvZ
526 R397H substitution alters the balance of porin production with down-regulation of the
527 major outer membrane pore, OmpF and up-regulation of the narrow outer membrane
528 pore, OmpC. EnvZ controls activity of OmpR, which is known to control the balance
529 of porin production as well as biofilm formation under low medium osmolarity
530 conditions (17,40). OmpF is well characterised as an entry point for β -lactams due to
531 the molecules' physiochemical properties, which makes entry possible through this
532 porin which has a larger pore size than OmpC (41,42). We showed that with OmpF
533 expression repressed, the cells are less permeable, leading to reduced levels of the
534 antibiotic in the cell and as a result decreased susceptibility. Whilst the EnvZ
535 substitution was selected in both planktonic and biofilm cultures only planktonic
536 cultures acquired the additional Q176K AcrB substitution, leading to even further
537 reduced drug accumulation and as a result, decreased susceptibility. To date, the
538 exact binding pocket responsible for recognition of cephalosporins, and β -lactams in
539 general, remains debatable with evidence pointing either to the proximal or the distal
540 binding pocket (25,43,44). Here, we showed that Q176K substitution is located in a

541 critically important position within the distal binding pocket of the protein, altering
542 significantly the binding dynamics of the pocket towards cephalosporins. We
543 hypothesise that this may lead to altered residence time in the pocket and result in
544 the observed macroscopic MDR effect. Significantly, our results are consistent with
545 prior data showing that Q176 is involved in substrate transport and coordination of
546 the chromogenic cephalosporin antibiotic nitrocefin in both docking and MD
547 simulation (25,29,45). Intriguingly, the orientation of cefotaxime in the binding pocket
548 was found to differ significantly from that of nitrocefin and cephalothin suggesting
549 multiple modes of β -lactam binding may exist within the distal binding pocket of AcrB
550 (Supplementary Figure S1, a-b, d).

551 Populations exposed to azithromycin also demonstrated a two-step selection, quickly
552 developing resistance to the drug with an 8-fold followed by a 16-fold increase in
553 azithromycin MIC. These changes were linked to two distinct amino acid
554 substitutions; AcrB R717L and RamR T18P. The AcrB substitution is located in the
555 proximal binding pocket, which is part of the principal drug entry and coordination
556 pathway for high molecular mass drugs and is predicted to impact substrate entry to
557 the pump. A role for R717 in the substrate pathway has previously been proposed
558 (29) and also shown to participate in the coordination of the related antibiotic,
559 rifampicin in at least one experimental structure (30). Docking of azithromycin into
560 the macrolide site A and B of the experimental structures, revealed that the R717 is
561 located far from the canonical site B, which is associated with erythromycin binding.
562 Therefore, this residue is more likely to participate in the earlier stages of the
563 substrate pathway in site A of the proximal pocket. Consistent with this interpretation,
564 we observed that the top docking pose of the azithromycin site A of the proximal
565 pocket brings it in direct contact with the R717 and as a result affected by the R717

566 substitution. This makes the pump more effective at exporting azithromycin out of the
567 cells and as a result, the population more resistant. The second substitution in RamR
568 resulted in the upregulation of this already “upgraded” AcrAB pump, leading to a 16x
569 rise in azithromycin MIC.

570 A small number of substitutions within AcrB have been identified and predicted to
571 change affinity for different drugs in the past (46). The substitutions identified in this
572 study have not been previously characterised for their role in resistance, which we
573 did here for the first time, providing strong genetic, phenotypic and structural
574 evidence for their functional impacts.

575 Both the mechanisms of resistance identified against azithromycin and cefotaxime
576 directly affect both membrane permeability and efflux activity of the cells. The nature
577 of these substitutions leads to cross-resistant phenotypes as accumulation of many
578 drugs is compromised by alterations of general porins and AcrAB. This is of critical
579 importance as exposure to a single drug can select for multi-drug resistant
580 populations with health-threatening implications.

581 We did however identify clear trade-offs between drug resistance and biofilm
582 formation. Although previous studies have associated exposure to sub-inhibitory
583 concentrations of azithromycin and cefotaxime with inhibition of biofilm formation
584 (47,48), the mechanisms identified in this study have not, to the best of our
585 knowledge, been associated with these antibiotics before. Although we showed that
586 biofilms respond and adapt to antibiotic stresses, we observed that this adaptation is
587 driven by the need to survive exposure to the drug and was not linked to biomass
588 production. Control biofilms passaged without stress made much larger biofilms over
589 time, but these improved biofilm forming lineages did not become more drug

590 resistant. To explore this surprising observation further, we grew biofilms of selected
591 strains representing a variety of biofilm formation and resistance phenotypes and
592 tested their ability to survive exposure to increasing ciprofloxacin concentrations. We
593 observed that only biofilms which had been exposed to ciprofloxacin were
594 significantly harder to kill. This reflects their possession of both a robust community
595 structure and drug-specific resistance mutations that makes them fitter in the specific
596 environment. Neither strains with increased resistance to ciprofloxacin but normal
597 biofilm capacity, nor those with normal drug sensitivity but increased biofilm capacity,
598 demonstrated a significant benefit when treated with ciprofloxacin. Based on these
599 results, we hypothesise that producing more biomass is not necessarily the best
600 solution to survive antibiotic exposure. Highly resistant biofilms may be more likely to
601 result from a combination of both structural and drug specific mechanisms.

602 Interestingly we did not identify mutations in pathways previously proposed to
603 contribute to persister cell formation, suggesting that these were not important in
604 adaption to the drug exposures in our experimental setup.

605 Biofilms play a crucial role in chronic infections and our observations suggested an
606 obvious fitness advantage of adapted biofilms over unexposed biofilm populations in
607 terms of drug resistance. To see if this impacts virulence we investigated the
608 pathogenicity of strains with different resistance and biofilm profiles, using the
609 *Galleria mellonella* infection model. We observed that mutations that rendered the
610 bacteria resistant to drugs had no significant impact on pathogenicity. However, the
611 biofilm ability of the strains was negatively correlated with pathogenicity, with strains
612 forming least biofilm being most virulent resulting in the lowest survival rates.

613 Having characterised a number of biofilm-related resistant phenotypes, we estimated
614 their stability in the absence of drug selective pressure using an accelerated biofilm
615 evolution experiment. Strains that had been exposed to ciprofloxacin and
616 azithromycin maintained their resistance profiles over extended passaging but
617 formed better biofilms. In contrast, cefotaxime exposed populations lost their
618 acquired resistance after a few passages whilst they became better biofilm formers.
619 This indicates that although stability of resistance is highly influenced by the nature
620 of the antimicrobial stress, bacteria can quickly adapt to a more sessile, community-
621 orientated lifestyle in the absence of drug. Analysis of azithromycin-exposed
622 populations which had improved their biofilm ability identified loss-of-function
623 mutations in cyclic di-GMP phosphodiesterase, YjcC. This is unsurprising as cyclic
624 di-GMP is well known for its role in biofilm formation in several organisms including
625 *Salmonella*, which harbours 12 proteins with GGDEF and 14 proteins with EAL
626 domains (49,50).

627 In conclusion we demonstrate here that biofilms are highly sensitive to stress from
628 low levels of antibiotics, rapidly adapt to drug pressure and that mechanisms of
629 resistance can incur costs to other important phenotypes. Using similar approaches
630 to those outlined here will help understand the impacts of drug exposure on biofilms
631 in many contexts. This can help inform how best to use antimicrobials and predict
632 how biofilms will respond to different stresses.

633 **Materials and methods**

634 *Biofilm adaptation and evolution model*

635 *Salmonella enterica* serovar Typhimurium 14028S was used as the parent strain to
636 initiate all biofilm experiments in this study. This strain has been used as a model for
637 *S. Typhimurium* biofilm studies by many groups including our own and has a fully
638 closed and annotated reference genome (Accession number: CP001363). To study
639 adaptation and evolution of *Salmonella* biofilms, we adapted a model described by
640 the Cooper group (11). Bacteria were grown on 6 mm soda lime glass beads (Sigma,
641 Z265950-1EA) for 72 hours in Lysogeny Broth (LB) with no salt. They were
642 incubated in glass universal tubes containing 5 mL of the medium in horizontal
643 position, with mild rocking at 40 rpm, at 30 °C. For each passage, the beads were
644 washed in PBS and transferred into fresh media with new sterile beads. The
645 experiment was carried out at the presence of three clinically-important antibiotics;
646 azithromycin, cefotaxime and ciprofloxacin at a final concentration of 10 µg/mL,
647 0.062 µg/mL and 0.015 µg/mL respectively. Eight independent lineages were
648 included per exposure; four drug-exposed biofilm lineages, two drug-exposed
649 planktonic cultures and two unexposed, bead-only control lineages. In each tube,
650 three initially sterile beads were used, one to be transferred to the next lineage, one
651 to be stored, and one from which cells were recovered for phenotyping. For storage,
652 one bead per passage was frozen in 20 % glycerol. For phenotyping, the cells were
653 isolated from the beads by vortexing in PBS for 30 seconds and then grown
654 overnight in 1 mL of LB broth, before being stored in chronological order in deep-well
655 plates in glycerol. The experiments were completed after 250 generations (17
656 passages) for the azithromycin and cefotaxime exposure and after 350 generations
657 (24 passages) for the ciprofloxacin exposure. Populations from an early (first

658 passage), middle (half way point lineage) and late (final passage) time point were
659 chosen for study and from each, three single colonies were isolated, sub-cultured
660 and stored in 20% glycerol. These single-cell isolates, and their parent populations
661 were stored in deep-well 96-well plates and used for phenotyping by replicating the
662 bacteria onto appropriate media to test for fitness, biofilm ability, morphology and
663 susceptibility (replication used 'QRep 96 Pin Replicators', Molecular devices X5054).
664 Figure 1 shows an overview of the experimental setup and phenotyping procedure.

665 *Model optimisation*

666 To determine the optimum culture conditions for achieving the greatest cell carriage
667 of *S. Typhimurium* 14028S biofilms on the glass beads, biofilms were grown in 5 mL
668 LB without salt on 6 mm glass beads at four standard microbiological incubation
669 temperatures: 25 °C, 30 °C, 37 °C and 40 °C. The cell counts on beads grown at
670 each temperature was determined every 24 hours for 96 hours. Biofilms were
671 washed in 1 mL PBS and harvested via vortexing for 30 seconds. The harvested
672 cells were serially diluted in a microtiter tray containing 180 µL PBS and 5 µL was
673 spotted onto a square LB agar plate. The number of colony forming units was
674 calculated and the incubation conditions yielding the greatest amount of cells was
675 determined.

676 *Crystal violet assay (CV)*

677 To measure biofilm formation, selected strains were grown overnight in LB broth and
678 then diluted into 200 µL of LB-NaCl to give an OD of 0.01 in microtiter plates. The
679 plates were incubated at 30 °C for 48 hours, covered in gas-permeable seals before
680 wells were emptied and vigorously rinsed with water before staining. For staining,
681 200 µL of 0.1% CV was added to each well and incubated for 15 minutes at room
682 temperature. The crystal violet dye was then removed, and the wells were rinsed

683 with water. The dye bound to the cells was then dissolved in 70% ethanol and the
684 absorbance was measured at 590 nm in a plate reader (FLUOStar Omega, BMG
685 Labtech).

686 *Biofilm morphology*

687 To visually assess biofilms morphology, we replicated isolates stored in 96 deep-well
688 plates on 1% agar LB-NaCl plates, supplemented with 40 µg/mL Congo red (CR)
689 dye. The strains of interest were diluted to a final OD of 0.01 in a microtiter plate and
690 were then printed on the Congo red plates. The plates were incubated for 48 hours
691 at 30 °C before being photographed to capture colony morphology.

692 *Antimicrobial susceptibility testing*

693 To determine the minimum inhibition concentrations of antimicrobials against strains
694 of interest, we used the broth microdilution method (51) and the agar dilution method
695 (13), following the EUCAST guidelines. In both cases, Mueller-Hinton broth or agar
696 was used. Changes of less than two dilutions were not considered significant.

697 *Molecular Modelling and Antibiotic Docking*

698 For docking analysis, protein and ligand PDB files were first converted to PDBqt
699 format using Raccoon (52). AutoDock Vina (53) was used for unbiased flexible
700 docking simulations of ligands on protein structures using an optimal box size,
701 estimated according to the radius of gyration of the ligands (grid-point spacing of 1
702 Å), centred on the predicted binding sites (supplementary table S1). The PyMOL
703 Molecular Graphics System, Version 2.0 Schrödinger, LLC. was used to visualize the
704 results. Formore information on model validation see supplementary materials.

705 *Extraction of DNA*

706 To extract genomic DNA for sequencing, selected strains were grown O/N in a 96-
707 deep-well plate in LB, at a final volume of 1.5 mL. Cells were recovered by
708 centrifugation at 3,500 g and were resuspended in 100 μ L of lysis buffer (5 μ g/mL
709 lysozyme, 0.1 mg/mL RNase in Tris-EDTA, pH 8) per well. The resuspended cells
710 were then transferred in a new semi-skirted, low-bind PCR plate, secured with an
711 adhesive seal and incubated at 37 °C, 1600 rpm for 25 minutes. 10 μ L of a lysis
712 additive buffer (5% SDS, 1 mg/mL proteinase K, 1 mg/mL RNase in Tris-EDTA, pH
713 8) was added in each well and the plate was sealed with PCR strip lids before being
714 incubated at 65 °C, 1600 rpm for 25 minutes. The plate was briefly centrifuged and
715 100 μ L were moved to a new PCR plate. For the DNA isolation, 50 μ L of DNA-
716 binding magnetic beads (KAPA Pure beads, Roche diagnostics) were added in each
717 well and were incubated at room temperature for 5 minutes. The plate was then
718 placed on a magnetic base and the supernatant was removed by pipetting. The
719 beads were washed three times with 80% freshly-prepared ethanol. After removing
720 the last wash, the beads were left to dry for 2 minutes before eluting the DNA. For
721 the DNA elution, the plate was removed from the magnetic apparatus and 50 μ L of
722 Tris-Cl were added to each well. The beads were pulled using the magnetic
723 apparatus and the isolated DNA was transferred to a new PCR plate. DNA
724 concentration was determined using the Qubit ds DNA HS Assay kit (Q32851)
725 following the manufacturer's instructions.

726 *Whole Genome sequencing*

727 Genomic DNA was normalised to 0.5 ng/ μ L with 10mM Tris-HCl. 0.9 μ L of TD
728 Tagment DNA Buffer (Illumina Catalogue No. 15027866) was mixed with 0.09 μ L
729 TDE1, Tagment DNA Enzyme (Illumina Catalogue No. 15027865) and 2.01 μ L PCR

730 grade water in a master mix and 3ul added to a chilled 96 well plate. 2 μ L of
731 normalised DNA (1ng total) was mixed with the 3 μ L of the tagmentation mix and
732 heated to 55 $^{\circ}$ C for 10 minutes in a PCR block. A PCR master mix was made up
733 using 4 ul kapa2G buffer, 0.4 μ L dNTP's, 0.08 μ L Polymerase and 4.52 μ L PCR
734 grade water, contained in the Kap2G Robust PCR kit (Sigma Catalogue No.
735 KK5005) per sample and 11 μ L added to each well need to be used in a 96-well
736 plate. 2 μ L of each P7 and P5 of Nextera XT Index Kit v2 index primers (Illumina
737 Catalogue No. FC-131-2001 to 2004) were added to each well. Finally, the 5 μ L
738 Tagmentation mix was added and mixed. The PCR was run with 72 $^{\circ}$ C for 3 minutes,
739 95 $^{\circ}$ C for 1 minute, 14 cycles of 95 $^{\circ}$ C for 10 seconds, 55 $^{\circ}$ C for 20 seconds and 72
740 $^{\circ}$ C for 3 minutes. Following the PCR reaction, the libraries were quantified using the
741 Quant-iT dsDNA Assay Kit, high sensitivity kit (Catalogue No. 10164582) and run on
742 a FLUOstar Optima plate reader. Libraries were pooled following quantification in
743 equal quantities. The final pool was double-spri size selected between 0.5 and 0.7X
744 bead volumes using KAPA Pure Beads (Roche Catalogue No. 07983298001). The
745 final pool was quantified on a Qubit 3.0 instrument and run on a High Sensitivity
746 D1000 ScreenTape (Agilent Catalogue No. 5067-5579) using the Agilent Tapestation
747 4200 to calculate the final library pool molarity. The pool was run at a final
748 concentration of 1.8 pM on an Illumina Nextseq500 instrument using a Mid Output
749 Flowcell (NSQ[®] 500 Mid Output KT v2(300 CYS) Illumina Catalogue FC-404-2003)
750 and 15 pM on a Illumina MiSeq instrument. Illumina recommended denaturation and
751 loading recommendations which included a 1% PhiX spike in (PhiX Control v3
752 Illumina Catalogue FC-110-3001). Whole genome sequencing data has been
753 deposited in the Sequence Read Archive under PRJNA529870.

754

755 *Bioinformatics*

756 Sequence reads from the sequencer were uploaded on to virtual machines provided
757 by the MRC CLIMB (Cloud Infrastructure for Microbial Bioinformatics) project using
758 BaseMount (54). Quality filtering of the sequence reads was performed using
759 Trimmomatic (version 3.5) with default parameters (55). Trimmomatic's Illuminaclip
760 function was used to remove the Illumina adapters. The trimmed reads were then
761 assembled into contigs using SPAdes version 3.11.1 using default parameters (56).

762 To determine single nucleotide polymorphisms (SNPs) between the de novo
763 assembled Salmonella genomes and the parent genome. Snippy version 3.1 was
764 used using parameters recommended in (<https://github.com/tseemann/snippy>). The
765 Snippy-core from the Snippy tool box was used to determine the core SNPs. The full
766 genome alignment output by Snippy-core was used in subsequent phylogenetic
767 analyses, after removal of the published reference sequence (accession number
768 CP001363). All 4870267 sites were included in the analysis to avoid ascertainment
769 bias (57). A whole-genome phylogenetic tree was then inferred from the 63
770 sequences under the model HKY+G implemented in iq-tree (58). For the individual
771 population analyses the control sequences were removed, the trees were estimated
772 with iq-tree, using the HKY+G evolutionary model. All trees were arbitrarily rooted at
773 the cultivated parental sequence 14028S for visualisation purposes, and were
774 plotted with ggtree for R (59). Branch lengths are given in units of substitutions/site.

775 *Preparation of RNA samples for q-RT PCR*

776 RNA from biofilms was isolated using the SV Total RNA Isolation System kit
777 (Promega). RNA was extracted from the WT (14028S), cef-biofilm-M-D-S1
778 (EnvZR397H), cef-plank-L-S2 (EnvZR397H/ AcrB Q176K), azi-biofilm-E-B-S2 (AcrB

779 R717L) and azi-biofilm-M-B-S1(AcrB R717L/ RamR T18P) strains. These were
780 grown O/N at 37 °C in LB and then spotted on LB-NaCl agar plates and were grown
781 for 48 hours at 30 °C. Cells from each spot were then resuspended in 100 µL TE
782 containing 50 mg/mL lysozyme and were homogenised by vortexing. 75 µL RNA
783 Lysis Buffer (Promega kit), followed by 350 µL RNA Dilution Buffer (Promega kit)
784 were added to the cell suspensions, which were then mixed by inversion. Samples
785 were incubated at 70 °C for 3 minutes and centrifuged at 13,000 g for 10 minutes.
786 The supernatant was mixed with 200 µL 95 % ethanol and was then loaded on to the
787 spin columns provided by the kit. The columns were washed with 600 µL RNA Wash
788 Solution. DNase mix was prepared following the Promega kit protocol and 50 µL
789 were directly added on the column membrane. After a 30 minutes incubation, 200 µL
790 DNase Stop Solution was added and samples were centrifuged for 30 seconds.
791 Columns were washed with 600 µL RNA Wash Solution followed by 250 µL RNA
792 Wash Solution, and then centrifuged again for 1 minute to dry. RNA was eluted using
793 100 µL of nuclease-free water. RNA quantification was performed using the Qubit
794 RNA High Sensitivity Assay kit (Q32852).

795 *Quantitative Real-Time PCR (q-RT PCR)*

796 To determine expression levels of *ompC/F*, *csgA/B* and *ramA*, we performed q-RT
797 PCR using the Luna Universal One-Step RT-qPCR Kit from NEB (E3005), using the
798 Applied Biosystems™ 7500 Real-Time PCR system. The primers used for the q-RT
799 PCR are listed in Table 2. Efficiency of the primers was calculated by generation of
800 calibration curves for each primer pair on serially diluted DNA samples. The R^2 of the
801 calibration curves calibrated was ≥ 0.98 for all the primer pairs used in this study.

802 RNA at a final amount of 50-100 ng was added to 10 µL final volume PCR reactions,
803 mixed with 400 nM of each primer. The cycle parameters were as follows: 10

804 minutes at 55 °C (reverse transcription step), 1-minute denaturation at 95 °C and 40
805 cycles of 10 seconds at 95 °C and 1 minute at 60 °C.

806 For each sample, two technical replicates from two biological replicates each were
807 included (four in total) per reaction. Controls with no reverse transcriptase were also
808 included for each RNA sample to eliminate DNA contamination.

809 To calculate expression levels, expression fold change was calculated using *gyrB*
810 expression as a reference. The relative expression was determined by calculating
811 the logarithmic base 2 of the difference between *gyrB* gene expression and target
812 gene expression per sample.

813 *Viability of cells within biofilms*

814 To determine the viability of cells within a biofilm, two approaches were used. The
815 first approach involved growing biofilms on glass beads for 72 hours. They were
816 washed in PBS to remove planktonic cells and were then challenged with different
817 concentrations of ciprofloxacin (0, 0.03, 0.3, 3 µg/mL) for 90 minutes. Beads were
818 washed again in PBS to remove any antibiotic and transferred into 1 mL of PBS
819 solution to an Eppendorf tube, where they were vigorously vortexed for 1 minute.
820 The cells recovered in PBS were serial diluted and spotted onto LB plates for CFU
821 counting the next day. For the second approach, we grew biofilms on glass slides for
822 72 hours. The slides were washed in PBS and were challenged with ciprofloxacin (3
823 µg/mL) for 90 minutes. They were washed in PBS and stained with a solution of 12
824 µM propidium iodide (PI) and 300 nM of SYTO 9 for 30 minutes. They were washed
825 in PBS and soaked in 70% ethanol to kill the cells before they were transferred to a
826 slide for microscopy. Fluorescence microscopy was performed in a Zeiss Axio
827 Imager M2.

828 *Galleria Infection model*

829 To test the pathogenicity of different mutants, we used the *Galleria mellonella* larvae
830 infection model. Wax worms were obtained from livefoods.co.uk. Similarly-sized
831 larvae with no signs of pupation or melanisation were chosen for injection. An initial
832 experiment was performed to calculate the infectious dose of *S. Typhimurium*
833 14028S in *G. mellonella*, which determined that an inoculation with approximately
834 20,000 CFU resulted in death of approximately half of 10 larvae after 72 hours. Once
835 this had been determined, overnight cultures of each strain were diluted in PBS to
836 replicate this inoculum concentration and 10 μ L of this were injected into the second
837 hindmost left proleg of ten larvae. To check the concentration of each inoculum, 100
838 μ L of each dilution were also plated onto LB agar and incubated overnight at 37°C.
839 CFUs were counted the next day and the inoculum concentration was confirmed.
840 Controls included in this experiment included larvae injected with PBS only and un-
841 injected larvae. All larvae were incubated at 37 °C and were checked three times a
842 day for 3 days to record the survival rate. The experiment was repeated on three
843 independent occasions, with 10 larvae randomly allocated per strain in each
844 experiment. Survival was calculated as the percentage of surviving larvae 48 hours
845 after injection (Figure 6, e).

846 *Cellular permeability assays*

847 To detect differences in cellular permeability to drugs between mutants, the
848 resazurin accumulation assay was used. The strains of interest were grown to
849 exponential phase, using a 1:100 inoculum from overnight cultures. The cells were
850 washed and resuspended in PBS normalising for cell density and they were mixed
851 with resazurin to a final volume of 100 μ L (to give 10 μ g/mL) in round-bottom
852 microtiter plates. Fluorescence was measured in the Omega FLUOstar plate reader

853 at excitation 544 nm and emission of 590 nm. Five replicates were included per
854 strain and resazurin-only reactions were used as controls. The assay was repeated
855 at least twice with reproducible results observed each time.

856 *Accelerated evolution experiments*

857 To test the phenotypic stability of strains recovered from the initial evolution
858 experiments, we performed an accelerated evolution experiment using six strains
859 representing a spectrum of biofilm forming capacities and drug resistance phenotypes
860 (WT, control-biofilm-L-S1, azi-biofilm-M-B-S2, azi-biofilm-M-B-S3, cef-biofilm-L-A-S1,
861 cip-biofilm-M-B-S2, cip-biofilm-L-B-S3). The strains were resuscitated from storage by
862 a 24-hour incubation at 37 °C in LB broth. After incubation, 50 µL of broth was added
863 to 5 mL of LB broth (without salt) containing three sterile glass beads and incubated
864 for 24 hours at 30 °C, until a biofilm was formed. Each bead was then washed in 1 mL
865 PBS to remove planktonic and loosely adherent cells. Two beads were stored in deep-
866 well plates containing 20 % glycerol for archiving and phenotyping. The third bead was
867 transferred to another tube of LB broth (without salt) containing three sterile glass
868 beads and passaged. This was repeated for ten passages, storing beads at each
869 timepoint.

870 Upon completion of ten passages, populations were recovered from passage five,
871 passage ten and the parental population for each mutant. From each population,
872 single colonies were picked after streaking out each population on LB agar and
873 incubating for 24 hours at 37 °C. Three colonies from each population were then
874 subcultured in LB broth. A population and three isolates from the start, middle and end
875 of the passage series were isolated and phenotyped for each mutant. Biofilm formation
876 was evaluated using the Congo Red and Crystal Violet assays. The agar dilution

877 methodology was used to assess the minimum inhibitory concentrations of antibiotics.
878 The average of the fold MIC change per antibiotic for all strains was calculated and
879 plotted against time. The average of biofilm formation, as determined by the crystal
880 violet assay, was calculated for all the strains per timepoint.

881 *Statistical analysis*

882 Biofilm forming ability was compared between strains or time points using linear mixed
883 models, with a random intercept of lineage where more than one lineage was included
884 for each strain or condition (Figures 1f and 6g).

885 Surviving cell counts were compared between strains using a linear mixed model with
886 a Poisson response, with random intercept of replicate, fixed effects of exposure, the
887 interaction between strain and exposure, and offset by the log of the average number
888 of cells counted in the 'unexposed' condition for each strain. Modelled means in each
889 exposure were then normalised by the average number of cells across all unexposed
890 conditions for plotting, such that the values shown represent the estimated proportion
891 of cells that would survive each exposure for each strain (Figure 6c). All error bars
892 reflect estimates +/- one standard error.

893 *Strains and genetic manipulations*

894 *Escherichia coli* DH10b was used as a host for all cloning procedures.

895 Transformations of *E. coli* were carried out by heat shock of chemically competent *E.*
896 *coli* cells. Transformation of *Salmonella* was carried out by electroporation.

897 *Salmonella* electrocompetent cells were prepared as follows: *Salmonella* cells were
898 grown to early exponential phase (OD_{600nm} 0.2-0.3) in 50 mL of 2x YT, using a 1:100
899 inoculum from an overnight culture. The cells were centrifuged and washed once

900 with filter sterilised ice-cold water. They were left to incubate on ice for 1 hour before
901 they were pelleted at 3,000 g for 15 minutes. The cell pellet was resuspended in 1
902 mL of 10% filter-sterilised glycerol and 100 μ L were used per transformation.

903 To create gene deletion mutants, we used the λ -red-based, gene doctoring
904 technique previously described in (60). For each deletion, two homologous regions
905 upstream and downstream of the genes of interest were amplified by PCR and were
906 cloned in MCS1 and MCS2 of the pDOC-K vector. The homologous regions were
907 300-400 bp in length and were designed to include the first and last 10 codons of the
908 gene to be deleted, to avoid any pleiotropic effects after deletion. For *acrB* and *ramR*
909 deletions, the upstream homologous regions were cloned EcoRI/ BamHI in MCS1
910 and the downstream ones as XhoI/ NheI in MCS2 of pDOC-K. For the *envZ* deletion,
911 the upstream homologous region was cloned EcoRI/ BamHI in MCS1 and the
912 downstream one as XhoI/ SpeI in MCS2.

913 For complementation of mutated genes, chromosomal integrations were created to
914 insert wild-type copies or mutated versions of genes of interest. This used a
915 modification of the gene doctoring system described above. pDOC-K was modified
916 to be used to deliver chromosomal gene integrations to the neutral intragenic region
917 downstream of *glms*. This chromosomal insertion site was proven to be neutral
918 through insertion of the reporter gene *lacZ*, where the mutant had no significant
919 difference in biofilm formation, efflux activity or competitive fitness (data not shown).

920 The integration vector (pDOC-K/ *glms*) was generated by cloning of the first
921 homologous region in MCS1 of pDOC-K, using EcoRI/ KpnI and the second
922 homologous region in MCS2 using XhoI/ NheI. The primer used for the amplification
923 of the second homologous region was designed to introduce a novel MCS (XhoI,
924 NdeI, SmaI, NotI, HindIII), upstream of the second homologous region which was

925 then used for the gene complementation constructs. Wild-type *ramR* and ‘*ramR*-
926 T18P’ alleles were cloned XhoI/ HindIII in pDOC-K/ glms under the control of the
927 gene’s native promoter. Wild-type *envZ* and ‘*envZ*-SNP’ alleles were cloned XhoI/
928 HindIII in pDOC-K/ glms under the control of a constitutive plac promoter. For *acrB*
929 complementation, we used the pWKS30/ AcrB plasmid previously described in (61),
930 expression of the gene is under the control of the pBAD system and induction was
931 achieved with the use of 0.5% arabinose.

932 For induction of chromosomal integrations either for deletion or complementation of
933 a gene, the strain to be modified was transformed with the pDOC-K vector variant
934 and the pACBSCE helper plasmid carrying the λ -red genes. A single colony carrying
935 both plasmids was grown in 500 μ L of LB, at 37 °C for 4 hours. The cells were
936 pelleted and washed three times in filter sterilized LB. They were then resuspended
937 in 500 μ L of 0.1x LB supplemented with 0.3% arabinose and incubated at 37 °C for
938 2-3 hours for induction. 100 μ L were plated on LB plates supplemented with 25 μ g/
939 mL kanamycin and 5% sucrose. The plates were incubated overnight at 37 °C.
940 Single colonies were checked for chromosomal alterations using colony PCR with
941 primers annealing outside of the region to be modified. The plasmids were removed
942 by sub culturing the positive clones on kanamycin-supplemented plates and testing
943 them for chloramphenicol and ampicillin sensitivity until the plasmids were
944 completely removed.

945 For ‘double deletions’ and/or complementations, the kanamycin cassette, introduced
946 by the first chromosomal modification, was removed using the FLP sites flanking the
947 cassette. The strains were transformed by electroporation with the pCP20 vector,
948 carrying the genes for flippase activity, and recovered on LB agar plates
949 supplemented with 50 μ g/mL ampicillin at 30 °C. The kanamycin cassette removal

950 was confirmed by colony PCR and the positive clones were sub-cultured on LB agar

951 at 37-42 °C. Removal of the plasmid was confirmed by testing the colonies'

952 sensitivity to ampicillin.

953

954 **Acknowledgements**

955 We would like to thank David Baker and Gemma Kay for assistance with sequencing and
956 Jacob Malone and Jessica Blair for helpful comments on the manuscript.

957 Funding

958 The author(s) gratefully acknowledge the support of the Biotechnology and Biological
959 Sciences Research Council (BBSRC); ET, AR, and MAW were supported by the BBSRC
960 Institute Strategic Programme Microbes in the Food Chain BB/R012504/1 and its constituent
961 project BBS/E/F/000PR10349. LOM and GS were supported by the Quadram Institute
962 Bioscience BBSRC funded Core Capability Grant (project number BB/CCG1860/1). V.N.B.
963 would like to acknowledge funding from Wellcome Trust grant 108372/A/15/Z and BBSRC
964 grant BB/N002776/1.

965 Transparency declaration

966 The funders had no role in study design, data collection and analysis, decision to publish, or
967 preparation of the manuscript

968 **References**

- 969 1. O'Neill J, The Review on Antimicrobial Resistance. Infection prevention, control
970 and surveillance: Limiting the development and spread of drug resistance.
971 London, UK; 2016 Mar.
- 972 2. Blair JMA, Webber MA, Baylay AJ, Ogbolu DO, Piddock LJV. Molecular
973 mechanisms of antibiotic resistance. *Nat Rev Microbiol*. 2015 Jan;13(1):42–51.
- 974 3. Webber MA, Whitehead RN, Mount M, Loman NJ, Pallen MJ, Piddock LJV.
975 Parallel evolutionary pathways to antibiotic resistance selected by biocide
976 exposure. *J Antimicrob Chemother*. 2015 Aug;70(8):2241–2248.
- 977 4. Hughes D, Andersson DI. Selection of resistance at lethal and non-lethal
978 antibiotic concentrations. *Curr Opin Microbiol*. 2012 Oct;15(5):555–560.
- 979 5. Marcusson LL, Frimodt-Møller N, Hughes D. Interplay in the selection of
980 fluoroquinolone resistance and bacterial fitness. *PLoS Pathog*. 2009 Aug
981 7;5(8):e1000541.
- 982 6. Costerton JW, Cheng KJ, Geesey GG, Ladd TI, Nickel JC, Dasgupta M, et al.
983 Bacterial biofilms in nature and disease. *Annu Rev Microbiol*. 1987;41:435–464.
- 984 7. Sauer K, Camper AK, Ehrlich GD, Costerton JW, Davies DG. *Pseudomonas*
985 *aeruginosa* displays multiple phenotypes during development as a biofilm. *J*
986 *Bacteriol*. 2002 Feb;184(4):1140–1154.
- 987 8. Miyaue S, Suzuki E, Komiyama Y, Kondo Y, Morikawa M, Maeda S. Bacterial
988 Memory of Persisters: Bacterial Persister Cells Can Retain Their Phenotype for
989 Days or Weeks After Withdrawal From Colony-Biofilm Culture. *Front Microbiol*.
990 2018 Jun 26;9:1396.
- 991 9. Cooper VS. Experimental Evolution as a High-Throughput Screen for Genetic
992 Adaptations. *mSphere*. 2018 Jun;3(3).
- 993 10. Martin M, Hölscher T, Dragoš A, Cooper VS, Kovács ÁT. Laboratory evolution
994 of microbial interactions in bacterial biofilms. *J Bacteriol*. 2016 Oct
995 1;198(19):2564–2571.
- 996 11. Poltak SR, Cooper VS. Ecological succession in long-term experimentally
997 evolved biofilms produces synergistic communities. *ISME J*. 2011
998 Mar;5(3):369–378.
- 999 12. Whitehead RN, Overton TW, Kemp CL, Webber MA. Exposure of *Salmonella*
1000 *enterica* serovar Typhimurium to high level biocide challenge can select
1001 multidrug resistant mutants in a single step. *PLoS One*. 2011 Jul
1002 29;6(7):e22833.

- 1003 13. Determination of minimum inhibitory concentrations (MICs) of antibacterial
1004 agents by agar dilution. *Clin Microbiol Infect.* 2000 Sep;6(9):509–515.
- 1005 14. Ostrer L, Khodursky RF, Johnson JR, Hiasa H, Khodursky A. Analysis of
1006 mutational patterns in quinolone resistance-determining regions of GyrA and
1007 ParC of clinical isolates. *Int J Antimicrob Agents.* 2018 Dec 21;
- 1008 15. Wang Y, Huang WM, Taylor DE. Cloning and nucleotide sequence of the
1009 *Campylobacter jejuni* gyrA gene and characterization of quinolone resistance
1010 mutations. *Antimicrob Agents Chemother.* 1993 Mar;37(3):457–463.
- 1011 16. Yoshida H, Bogaki M, Nakamura M, Nakamura S. Quinolone resistance-
1012 determining region in the DNA gyrase gyrA gene of *Escherichia coli*. *Antimicrob*
1013 *Agents Chemother.* 1990 Jun;34(6):1271–1272.
- 1014 17. Cai SJ, Inouye M. EnvZ-OmpR interaction and osmoregulation in *Escherichia*
1015 *coli*. *J Biol Chem.* 2002 Jul 5;277(27):24155–24161.
- 1016 18. Tipton KA, Rather PN. An ompR-envZ Two-Component System Ortholog
1017 Regulates Phase Variation, Osmotic Tolerance, Motility, and Virulence in
1018 *Acinetobacter baumannii* Strain AB5075. *J Bacteriol.* 2017 Feb 1;199(3).
- 1019 19. Jubelin G, Vianney A, Beloin C, Ghigo J-M, Lazzaroni J-C, Lejeune P, et al.
1020 CpxR/OmpR interplay regulates curli gene expression in response to osmolarity
1021 in *Escherichia coli*. *J Bacteriol.* 2005 Mar;187(6):2038–2049.
- 1022 20. Martínez-Martínez L, Conejo MC, Pascual A, Hernández-Allés S, Ballesta S,
1023 Ramírez De Arellano-Ramos E, et al. Activities of imipenem and
1024 cephalosporins against clonally related strains of *Escherichia coli*
1025 hyperproducing chromosomal beta-lactamase and showing altered porin
1026 profiles. *Antimicrob Agents Chemother.* 2000 Sep;44(9):2534–2536.
- 1027 21. Lovelle M, Mach T, Mahendran KR, Weingart H, Winterhalter M, Gameiro P.
1028 Interaction of cephalosporins with outer membrane channels of *Escherichia*
1029 *coli*. Revealing binding by fluorescence quenching and ion conductance
1030 fluctuations. *Phys Chem Chem Phys.* 2011 Jan 28;13(4):1521–1530.
- 1031 22. Nikaido H. Crossing the envelope: how cephalosporins reach their targets. *Clin*
1032 *Microbiol Infect.* 2000;6 Suppl 3:22–26.
- 1033 23. Prigent-Combaret C, Brombacher E, Vidal O, Ambert A, Lejeune P, Landini P,
1034 et al. Complex regulatory network controls initial adhesion and biofilm formation
1035 in *Escherichia coli* via regulation of the csgD gene. *J Bacteriol.* 2001
1036 Dec;183(24):7213–7223.
- 1037 24. Pos KM. Drug transport mechanism of the AcrB efflux pump. *Biochim Biophys*
1038 *Acta.* 2009 May;1794(5):782–793.

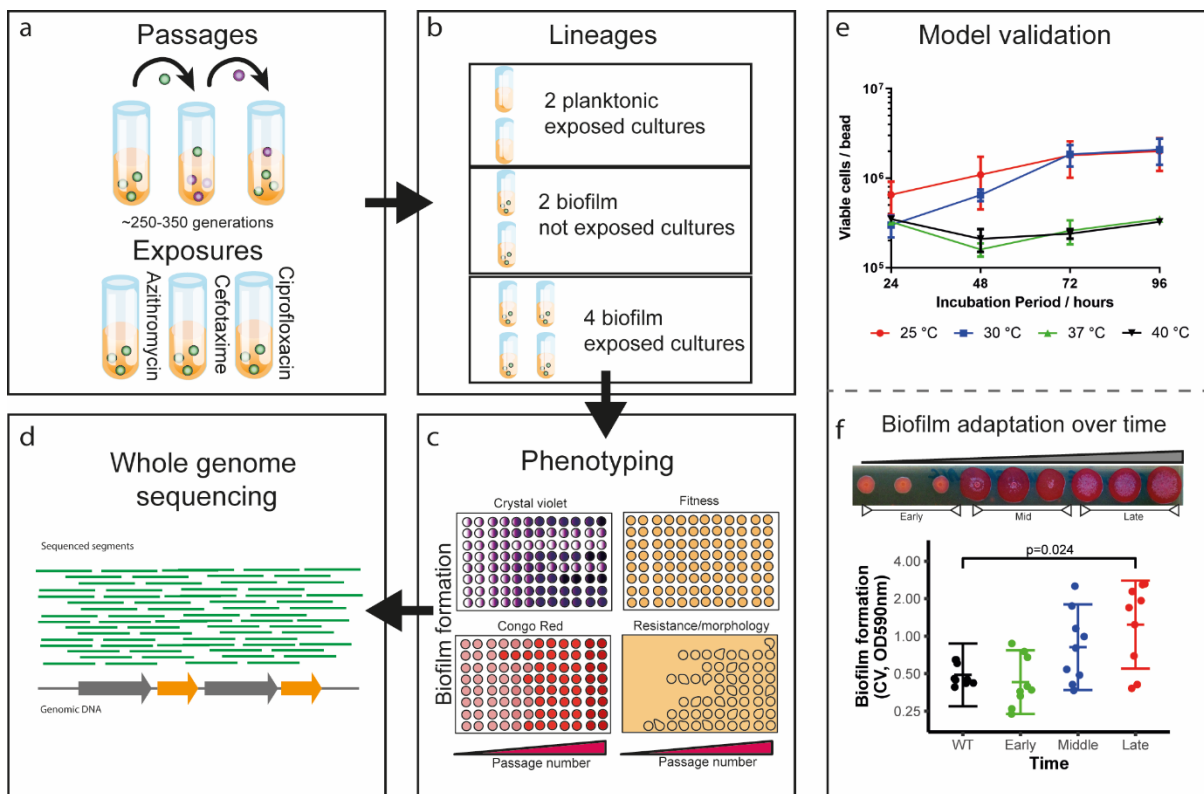
- 1039 25. Vargiu AV, Nikaido H. Multidrug binding properties of the AcrB efflux pump
1040 characterized by molecular dynamics simulations. *Proc Natl Acad Sci USA*.
1041 2012 Dec 11;109(50):20637–20642.
- 1042 26. Nikaido H, Pagès J-M. Broad-specificity efflux pumps and their role in multidrug
1043 resistance of Gram-negative bacteria. *FEMS Microbiol Rev*. 2012
1044 Mar;36(2):340–363.
- 1045 27. Murakami S, Nakashima R, Yamashita E, Matsumoto T, Yamaguchi A. Crystal
1046 structures of a multidrug transporter reveal a functionally rotating mechanism.
1047 *Nature*. 2006 Sep 14;443(7108):173–179.
- 1048 28. Sjölund-Karlsson M, Joyce K, Blickenstaff K, Ball T, Haro J, Medalla FM, et al.
1049 Antimicrobial susceptibility to azithromycin among *Salmonella enterica* isolates
1050 from the United States. *Antimicrob Agents Chemother*. 2011 Sep;55(9):3985–
1051 3989.
- 1052 29. Husain F, Nikaido H. Substrate path in the AcrB multidrug efflux pump of
1053 *Escherichia coli*. *Mol Microbiol*. 2010 Oct;78(2):320–330.
- 1054 30. Nakashima R, Sakurai K, Yamasaki S, Nishino K, Yamaguchi A. Structures of
1055 the multidrug exporter AcrB reveal a proximal multisite drug-binding pocket.
1056 *Nature*. 2011 Nov 27;480(7378):565–569.
- 1057 31. Yamasaki S, Nikaido E, Nakashima R, Sakurai K, Fujiwara D, Fujii I, et al. The
1058 crystal structure of multidrug-resistance regulator RamR with multiple drugs.
1059 *Nat Commun*. 2013;4:2078.
- 1060 32. Abouzeed YM, Baucheron S, Cloeckert A. ramR mutations involved in efflux-
1061 mediated multidrug resistance in *Salmonella enterica* serovar Typhimurium.
1062 *Antimicrob Agents Chemother*. 2008 Jul;52(7):2428–2434.
- 1063 33. Eicher T, Cha H, Seeger MA, Brandstätter L, El-Delik J, Bohnert JA, et al.
1064 Transport of drugs by the multidrug transporter AcrB involves an access and a
1065 deep binding pocket that are separated by a switch-loop. *Proc Natl Acad Sci*
1066 *USA*. 2012 Apr 10;109(15):5687–5692.
- 1067 34. Santos-Lopez A, Marshall CW, Scribner MR, Snyder D, Cooper VS. Biofilm-
1068 dependent evolutionary pathways to antibiotic resistance. *BioRxiv*. 2019 Mar
1069 19;
- 1070 35. Høiby N, Bjarnsholt T, Givskov M, Molin S, Ciofu O. Antibiotic resistance of
1071 bacterial biofilms. *Int J Antimicrob Agents*. 2010 Apr;35(4):322–332.
- 1072 36. Stewart PS. Theoretical aspects of antibiotic diffusion into microbial biofilms.
1073 *Antimicrob Agents Chemother*. 1996 Nov;40(11):2517–2522.

- 1074 37. Anderl JN, Franklin MJ, Stewart PS. Role of antibiotic penetration limitation in
1075 *Klebsiella pneumoniae* biofilm resistance to ampicillin and ciprofloxacin.
1076 *Antimicrob Agents Chemother.* 2000 Jul;44(7):1818–1824.
- 1077 38. de la Fuente-Núñez C, Reffuveille F, Fernández L, Hancock REW. Bacterial
1078 biofilm development as a multicellular adaptation: antibiotic resistance and new
1079 therapeutic strategies. *Curr Opin Microbiol.* 2013 Oct;16(5):580–589.
- 1080 39. Mah TF, O’Toole GA. Mechanisms of biofilm resistance to antimicrobial agents.
1081 *Trends Microbiol.* 2001 Jan;9(1):34–39.
- 1082 40. Silva IN, Pessoa FD, Ramires MJ, Santos MR, Becker JD, Cooper VS, et al.
1083 The OmpR Regulator of *Burkholderia multivorans* Controls Mucoid-to-
1084 Nonmucoid Transition and Other Cell Envelope Properties Associated with
1085 Persistence in the Cystic Fibrosis Lung. *J Bacteriol.* 2018 Sep 1;200(17).
- 1086 41. Benz R, Schmid A, Hancock RE. Ion selectivity of gram-negative bacterial
1087 porins. *J Bacteriol.* 1985 May;162(2):722–727.
- 1088 42. Masi M, Réfregiers M, Pos KM, Pagès J-M. Mechanisms of envelope
1089 permeability and antibiotic influx and efflux in Gram-negative bacteria. *Nat*
1090 *Microbiol.* 2017 Feb 22;2:17001.
- 1091 43. Kobayashi N, Tamura N, van Veen HW, Yamaguchi A, Murakami S. β -Lactam
1092 selectivity of multidrug transporters AcrB and AcrD resides in the proximal
1093 binding pocket. *J Biol Chem.* 2014 Apr 11;289(15):10680–10690.
- 1094 44. Yu EW, Aires JR, McDermott G, Nikaido H. A periplasmic drug-binding site of
1095 the AcrB multidrug efflux pump: a crystallographic and site-directed
1096 mutagenesis study. *J Bacteriol.* 2005 Oct;187(19):6804–6815.
- 1097 45. Takatsuka Y, Chen C, Nikaido H. Mechanism of recognition of compounds of
1098 diverse structures by the multidrug efflux pump AcrB of *Escherichia coli*. *Proc*
1099 *Natl Acad Sci USA.* 2010 Apr 13;107(15):6559–6565.
- 1100 46. Blair JMA, Bavro VN, Ricci V, Modi N, Cacciotto P, Kleinekathöfer U, et al.
1101 AcrB drug-binding pocket substitution confers clinically relevant resistance and
1102 altered substrate specificity. *Proc Natl Acad Sci USA.* 2015 Mar
1103 17;112(11):3511–3516.
- 1104 47. Wang A, Wang Q, Kudinha T, Xiao S, Zhuo C. Effects of Fluoroquinolones and
1105 Azithromycin on Biofilm Formation of *Stenotrophomonas maltophilia*. *Sci Rep.*
1106 2016 Jul 13;6(1):29701.
- 1107 48. Baothong S, Sitthisak S, Kunthalert D. In vitro interference of cefotaxime at
1108 subinhibitory concentrations on biofilm formation by nontypeable *Haemophilus*
1109 *influenzae*. *Asian Pac J Trop Biomed.* 2016 Sep;6(9):745–750.

- 1110 49. Simm R, Morr M, Kader A, Nimtz M, Römling U. GGDEF and EAL domains
1111 inversely regulate cyclic di-GMP levels and transition from sessility to motility.
1112 Mol Microbiol. 2004 Aug;53(4):1123–1134.
- 1113 50. Ahmad I, Lamprokostopoulou A, Le Guyon S, Streck E, Barthel M, Peters V, et
1114 al. Complex c-di-GMP signaling networks mediate transition between virulence
1115 properties and biofilm formation in *Salmonella enterica* serovar Typhimurium.
1116 PLoS One. 2011 Dec 2;6(12):e28351.
- 1117 51. EUCAST reading guide for broth microdilution.
- 1118 52. Forli S, Huey R, Pique ME, Sanner MF, Goodsell DS, Olson AJ. Computational
1119 protein-ligand docking and virtual drug screening with the AutoDock suite. Nat
1120 Protoc. 2016 May;11(5):905–919.
- 1121 53. Trott O, Olson AJ. AutoDock Vina: improving the speed and accuracy of
1122 docking with a new scoring function, efficient optimization, and multithreading. J
1123 Comput Chem. 2010 Jan 30;31(2):455–461.
- 1124 54. Connor TR, Loman NJ, Thompson S, Smith A, Southgate J, Poplawski R, et al.
1125 CLIMB (the Cloud Infrastructure for Microbial Bioinformatics): an online
1126 resource for the medical microbiology community. Microb Genom. 2016 Sep
1127 20;2(9):e000086.
- 1128 55. Bolger AM, Lohse M, Usadel B. Trimmomatic: a flexible trimmer for Illumina
1129 sequence data. Bioinformatics. 2014 Aug 1;30(15):2114–2120.
- 1130 56. Nurk S, Bankevich A, Antipov D, Gurevich A, Korobeynikov A, Lapidus A, et al.
1131 Assembling Genomes and Mini-metagenomes from Highly Chimeric Reads. In:
1132 Deng M, Jiang R, Sun F, Zhang X, editors. Research in computational
1133 molecular biology. Berlin, Heidelberg: Springer Berlin Heidelberg; 2013. p. 158–
1134 170.
- 1135 57. Tamuri A, Goldman N. Avoiding ascertainment bias in the maximum likelihood
1136 inference of phylogenies based on truncated data. BioRxiv. 2017 Sep 9;
- 1137 58. Nguyen L-T, Schmidt HA, von Haeseler A, Minh BQ. IQ-TREE: a fast and
1138 effective stochastic algorithm for estimating maximum-likelihood phylogenies.
1139 Mol Biol Evol. 2015 Jan;32(1):268–274.
- 1140 59. Yu G, Smith DK, Zhu H, Guan Y, Lam TT-Y. *ggtree*: an R package for
1141 visualization and annotation of phylogenetic trees with their covariates and
1142 other associated data. Methods Ecol Evol. 2016 Aug;
- 1143 60. Lee DJ, Bingle LEH, Heurlier K, Pallen MJ, Penn CW, Busby SJW, et al. Gene
1144 doctoring: a method for recombineering in laboratory and pathogenic
1145 *Escherichia coli* strains. BMC Microbiol. 2009 Dec 9;9:252.

- 1146 61. Baugh S, Ekanayaka AS, Piddock LJV, Webber MA. Loss of or inhibition of all
1147 multidrug resistance efflux pumps of *Salmonella enterica* serovar Typhimurium
1148 results in impaired ability to form a biofilm. *J Antimicrob Chemother.* 2012
1149 Oct;67(10):2409–2417.
- 1150 62. Jarvik T, Smillie C, Groisman EA, Ochman H. Short-term signatures of
1151 evolutionary change in the *Salmonella enterica* serovar typhimurium 14028
1152 genome. *J Bacteriol.* 2010 Jan;192(2):560–567.
- 1153

1154 **Figures**



1155

1156 **Figure 1: Salmonella biofilm adaptation model.** **a**, Sterile glass beads were used
 1157 for the establishment of Salmonella biofilms. Three antibiotics were selected and used
 1158 as stressors; azithromycin, cefotaxime and ciprofloxacin. **b**, For each experiment,
 1159 eight independent lineages were ran in parallel; two planktonic controls, exposed to
 1160 the drug, with no beads present; two bead controls, not exposed to the drug, and four
 1161 independent lineages, exposed to the drug on beads. **c**, Passages and sampling were
 1162 carried out every 72 hours at 30 °C and the cells isolated were stored and phenotyped
 1163 for biofilm formation, fitness, susceptibility etc. **d**, Over 100 strains (populations and
 1164 single-cell isolates) were selected and sequenced based on their phenotypic
 1165 characteristics. **e**, To determine the right experimental conditions for the evolution
 1166 experiment, cells were recovered and counted from biofilms grown for different periods
 1167 of time, at different temperatures. This showed that the maximum cell carriage is
 1168 achieved by 72 h at either 25 °C or 30 °C. Dots indicate average from 4 replicates and
 1169 error bars show standard error. **f**, To determine whether bacteria adapt to the bead
 1170 model, biofilm formation was monitored over time by visualisation on Congo red-
 1171 supplemented plates and by the Crystal Violet assay (OD:590nm), using the
 1172 unexposed bead control lineages. The strains quickly adapted and produced
 1173 significantly more biomass compared to the WT by the end of the experiment. Each
 1174 dot represents single cell strains isolated from different timepoints. Error bars reflect
 1175 estimated +/- one standard error.

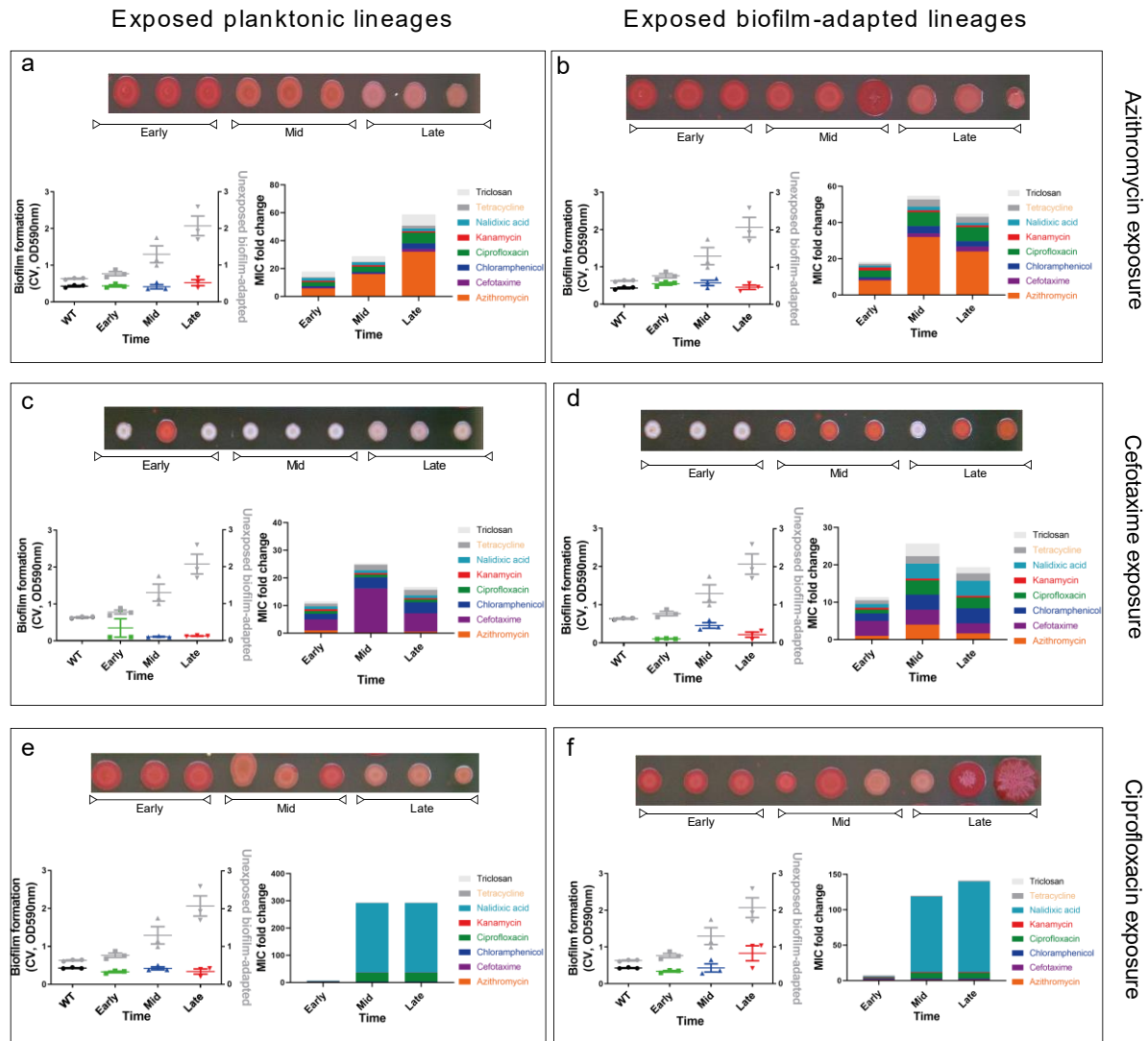
1176

1177

1178

1179

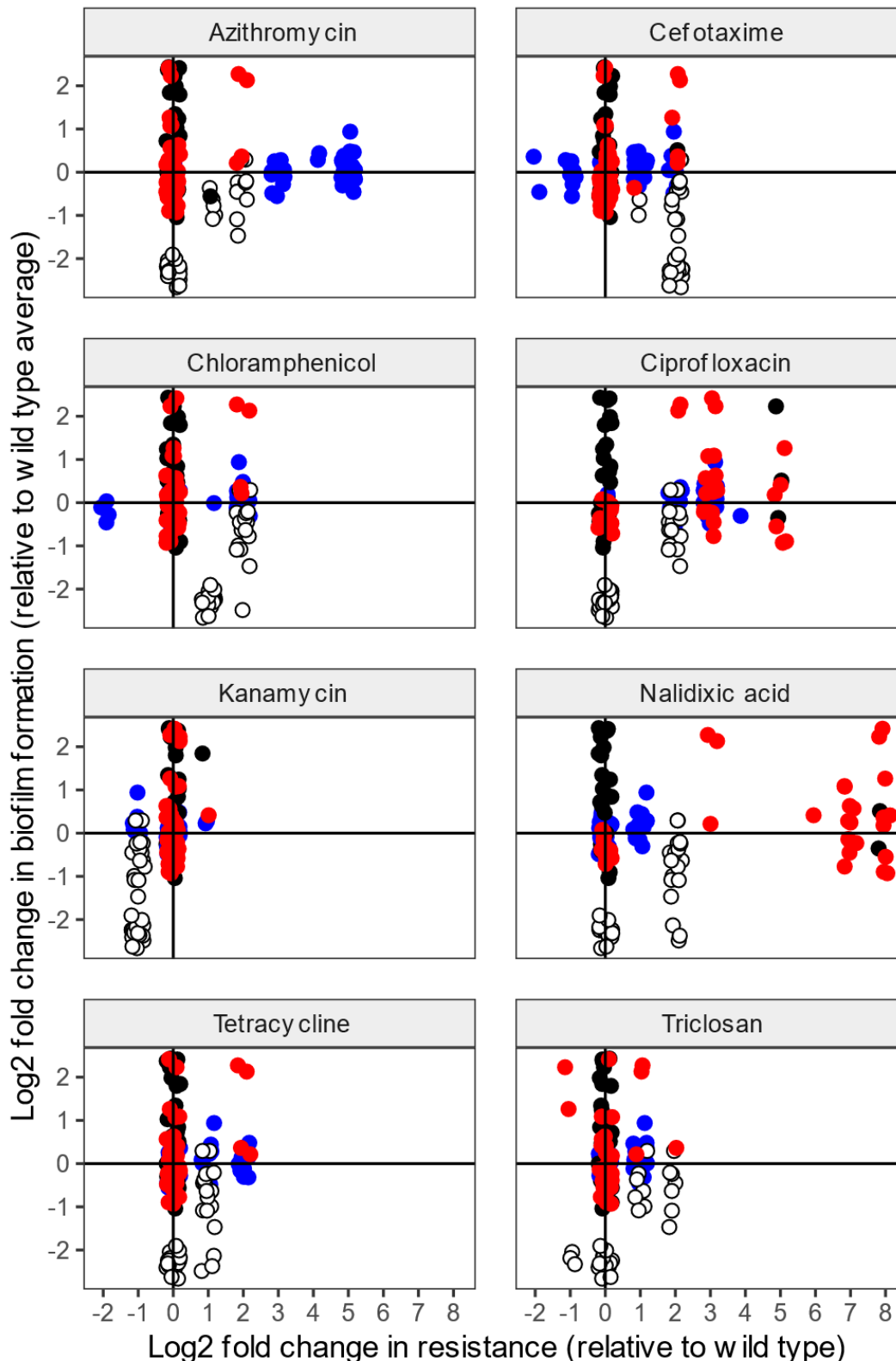
1180



1181
1182
1183
1184
1185
1186
1187
1188
1189
1190
1191
1192
1193
1194
1195
1196
1197
1198
1199
1200
1201

Figure 2: Biofilms adapt to antibiotic stress, with diverse effects on biofilm formation. Planktonic and biofilm populations, exposed to azithromycin (a-b), cefotaxime (c-d) and ciprofloxacin (e-f) were isolated at different timepoints during the evolution experiment (early, mid, late). Panels on the left show data from planktonic lineages, panels on the right from biofilm lineages. Three single isolates per timepoint were tested for their biofilm ability and susceptibility. Biofilm formation was measured by the Crystal Violet assay and on Congo Red plates. Unexposed biofilm lineages were used as a reference to biofilm adaptation (results shown in grey on CV graphs). Antibiotic susceptibility was determined by measuring the MIC values for a panel of different antimicrobials (azithromycin, cefotaxime, chloramphenicol, ciprofloxacin, kanamycin, nalidixic acid, tetracycline and triclosan). Stacked bars were generated by stacking the average MICs for each antibiotic (colour-coded), from three single cell isolates a-b, Both planktonic and biofilm isolates, exposed to azithromycin, developed resistance to azithromycin as well as decreased susceptibility to cefotaxime, chloramphenicol, ciprofloxacin, nalidixic acid, tetracycline and triclosan. Biofilm adaptation was inhibited in the biofilm lineages. c-d, Planktonic lineages, exposed to cefotaxime, rapidly developed resistance to cefotaxime. Biofilms under the same exposure exhibited an MDR response. Biofilm adaptation of both planktonic and biofilm lineages was completely compromised leading to pale colonies on CR plates. e-f, Planktonic and biofilm lineages exposed to ciprofloxacin adapted to the stress by

1202 *developing resistance to the stressor. Biofilm adaptation was delayed compared to the*
1203 *unexposed control lineages but significantly increased by the end of the experiment.*
1204



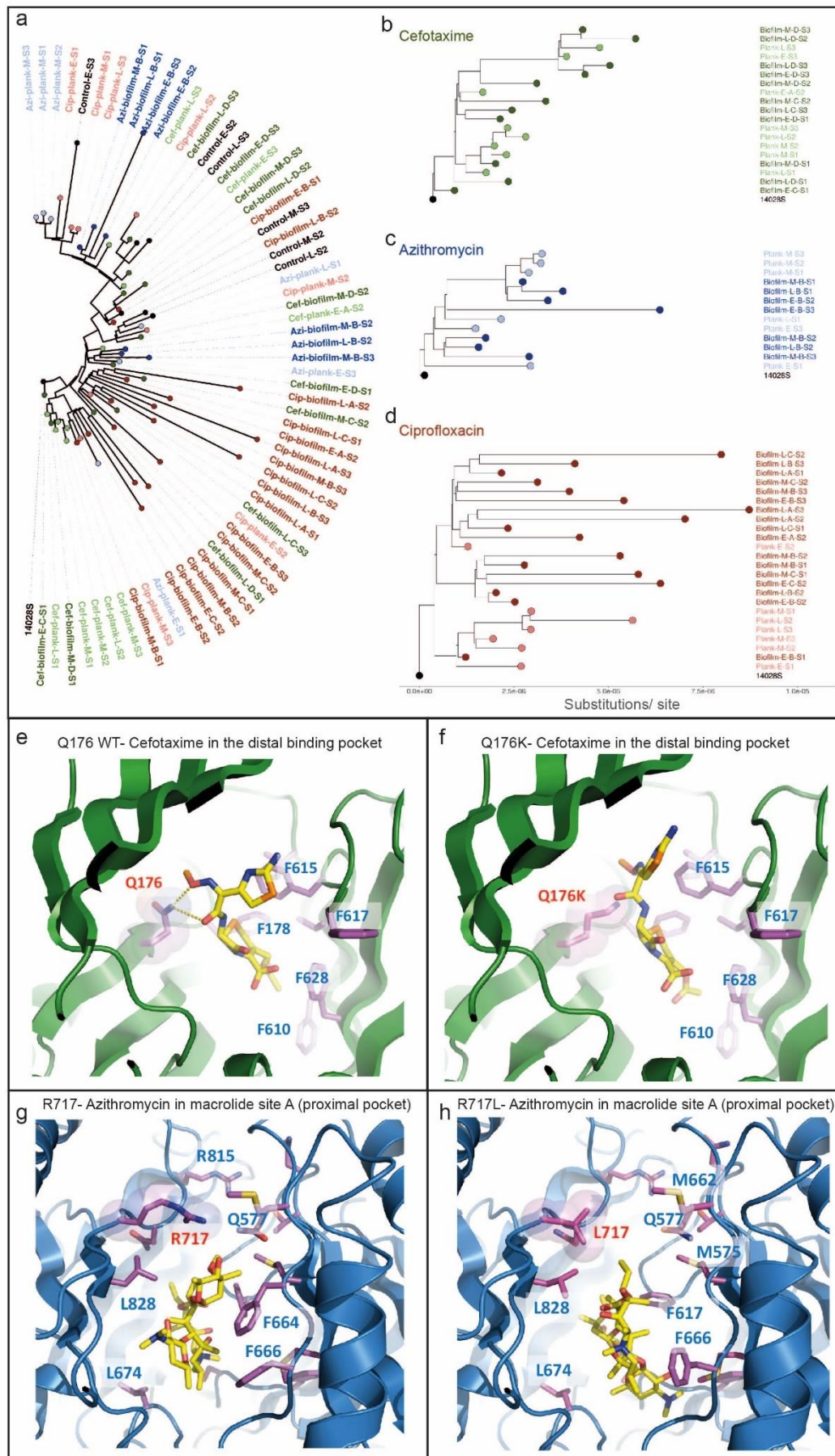
1205 **Figure 3: Correlations between resistance and biofilm formation selected by**
1206 **different antibiotics. a-h,** Fold change in MIC for each antibiotic was compared
1207 against the fold change in biofilm formation. Single isolates were characterised; with
1208 each dot on the graphs representing an individual isolate from each evolution
1209 experiment (blue: azithromycin, white: cefotaxime, red: ciprofloxacin, black: drug-free
1210 controls). The parent strain average, used as a reference, is represented as point '0,0'

1211 *on the graphs. Azithromycin and cefotaxime exposed isolates became less*
1212 *susceptible not only to the stressor but also to other antimicrobials. Ciprofloxacin-*
1213 *exposed isolates only became resistant to fluoroquinolones. Biofilm formation was*
1214 *heavily compromised in cefotaxime-exposed strains. Azithromycin inhibited biofilm*
1215 *formation with some strains exhibiting slightly reduced levels of biofilm formation,*
1216 *whereas ciprofloxacin did not have a significant effect on biofilm adaptation.*

1217

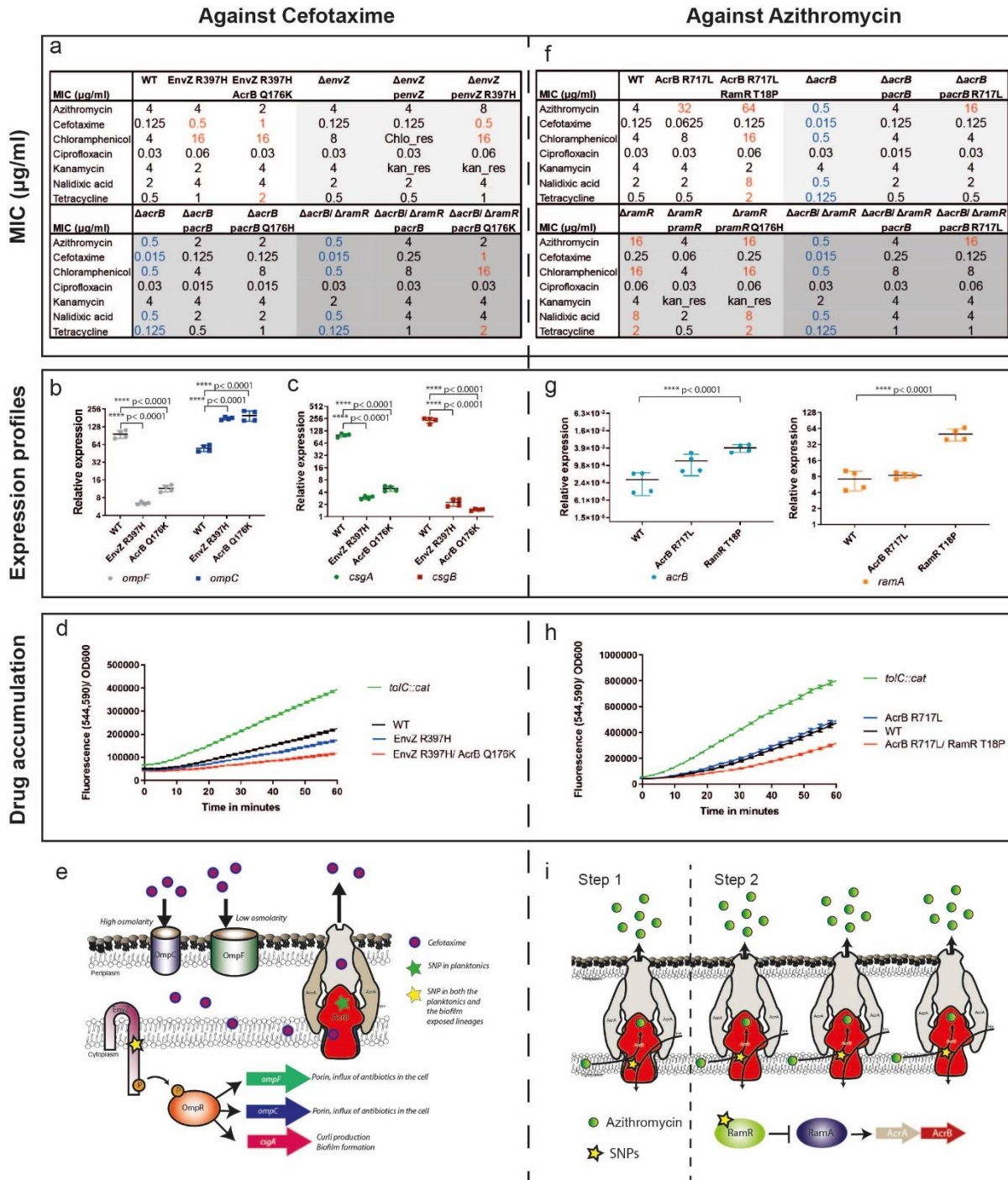
1218

1219



1220 **Figure 4. Phylogenetic analysis and AcrB modelling. a**, Universal phylogenetic
1221 tree based on full genome alignment, showing diversity of strains exposed to
1222 azithromycin, cefotaxime and ciprofloxacin. Azithromycin and cefotaxime selected for
1223 mutants that followed a distinct evolution pattern, whereas ciprofloxacin-exposed
1224 strains evolved and responded to the stress in various ways. *S. Typhimurium*
1225 14028S (CP001363) was used as the reference strain and the tree was arbitrarily
1226 rooted at the cultivated parental sequence 14028S. **b-d**, Individual trees were
1227 generated for cefotaxime, azithromycin and ciprofloxacin-exposed strains. Dark dots
1228 indicate biofilm lineages, light dots planktonic lineages. Phylogenetic variations
1229 between biofilms and planktonic cultures were observed, indicating unique
1230 mechanisms of resistance between the two states. **e**, Cefotaxime binding to the
1231 distal binding pocket of AcrB (4DX5, chain B). Q176 is involved in the coordination of
1232 cephalosporin molecules in the binding pocket. **f**, Upon substitution with lysine
1233 (Q176K), the free energy of binding changed significantly, potentially resulting in
1234 reduced residence time of the drug in the pocket and hence, increased efflux **g**,
1235 Azithromycin docking to macrolide site A of the proximal binding pocket of AcrB
1236 (3AOB, chain C). R717 exhibits a direct involvement in macrolide coordination in the
1237 pocket. **h**, Substitution with leucine (R717L) led to radically altered coordination of
1238 azithromycin in the pocket.

1239



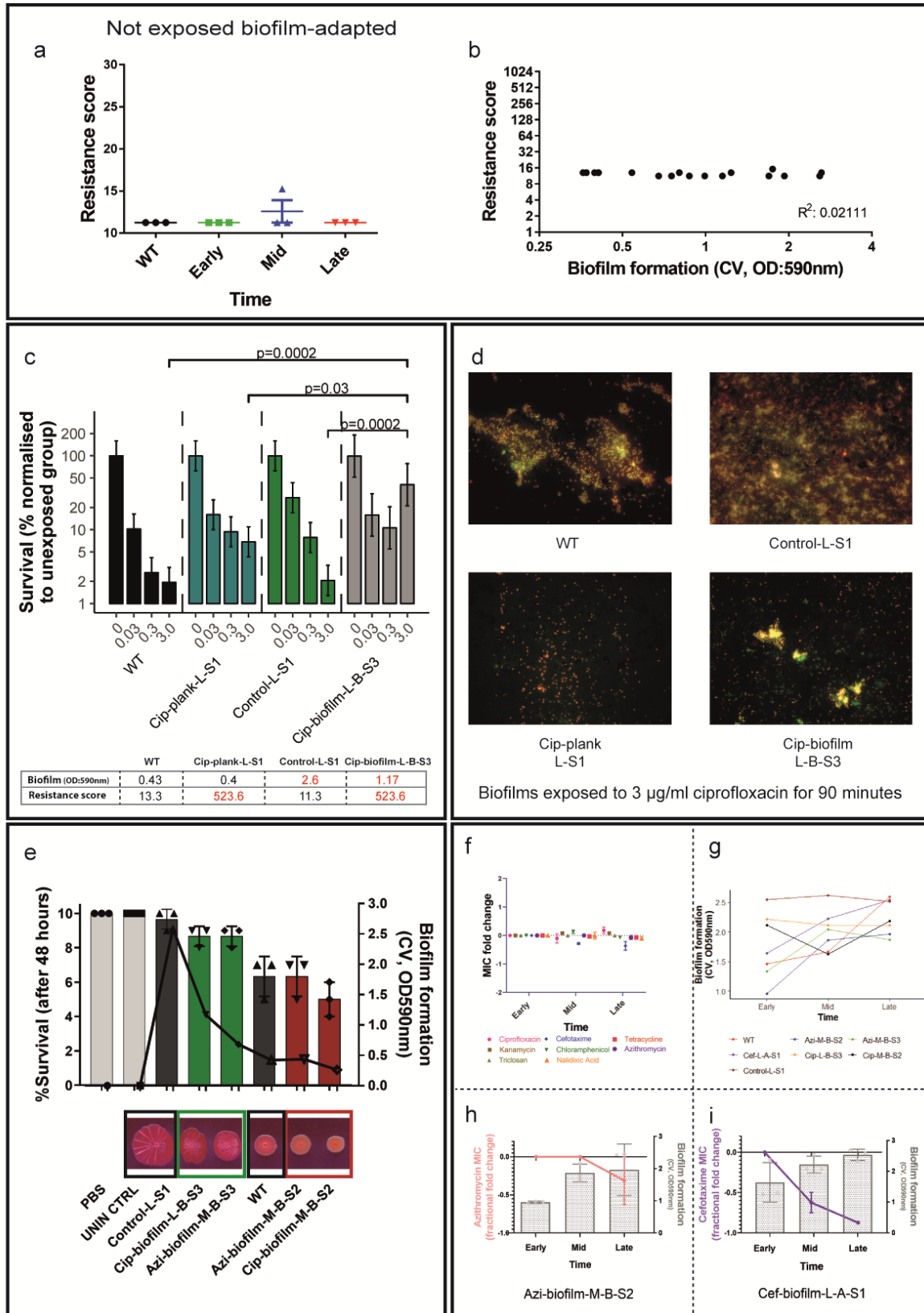
1240

1241 **Figure 5: Proposed novel mechanism of resistance to cefotaxime and**
 1242 **azithromycin. a-i,** Cefotaxime and azithromycin exposed isolates exhibiting decreased
 1243 susceptibility, were whole-genome-sequenced and genetic variations were identified. **a,**
 1244 Cefotaxime exposed isolates from the middle timepoint carried the R397H substitution in
 1245 EnvZ leading to reduced susceptibility to cefotaxime and chloramphenicol. Isolates from the
 1246 late timepoint carried an additional Q176H substitution in AcrB (efflux pump). This resulted in
 1247 an increase in MIC for both cefotaxime and chloramphenicol as well as tetracycline. Deletion
 1248 and complementation of WT envZ had no effect on resistance while complementation with
 1249 the R397H variant, reproduced the resistance results from the isolated strain. Deletion of

1250 *acrB* led to increased susceptibility against all efflux substrate antibiotics. Complementation
1251 with *AcrB* Q176K variant, in the Δ *AcrB*/ Δ *RamR* background, resulted in complete recovery
1252 of the resistant phenotype. **b**, q RT-PCR from 48-hour biofilms, using *gyrB* as a reference,
1253 resulted in significantly reduced *ompF* (large porin) expression, whereas *ompC* (narrow
1254 porin) expression significantly increased. **c**, Expression of *csgA/B* (main curli subunits) was
1255 abolished, explaining the pale morphotype cefotaxime-resistant-mutants exhibited. **d**, To test
1256 whether the changes on porin composition affect membrane permeability, drug accumulation
1257 was measured using the resazurin assay. A *tolC::cat*, pump-defective mutant, was used as a
1258 control. Both resistant mutants exhibited decreased drug accumulation, reflective of the
1259 altered membrane composition. **e**, Resistance against cefotaxime is a synergistic result of
1260 reduced membrane permeability due to porin alterations and increased efflux through the
1261 *AcrA/B-TolC* pump. **f**, Azithromycin exposed strains, from an early time point, obtained an
1262 *AcrB* R717L substitution which led to an 8-fold increase in azithromycin MIC. At a later
1263 stage, an additional substitution in *RamR* (T18P) emerged. This resulted in an MDR
1264 phenotype with increased MICs of azithromycin, chloramphenicol, nalidixic acid and
1265 tetracycline. Complementation of *AcrB* R717L in the Δ *AcrB* and of the *RamR* T18P in the
1266 Δ *RamR* background reproduced the resistance profiles of the strains isolated from the
1267 evolution experiments, confirming that these substitutions are responsible for the resistant
1268 phenotypes observed. **g**, Expression of *acrB* and *ramA* were monitored by q RT-PCR in 48-
1269 hour biofilms and showed increased expression of both *acrB* and *ramA* in the isolate
1270 carrying the *RamR* T18P substitution. **h**, Membrane permeability was monitored by the
1271 resazurin assay and reduced accumulation was observed because of the *RamR* T18P
1272 substitution, which potentially leads to overexpression of the RND pump. **i**, Resistance
1273 against azithromycin is a result of the modification of the *AcrA/B-TolC* pump, leading to
1274 increased efflux and overexpression of it due to the absence of negative regulation in the
1275 *RamR* T18P substitution strain.

1276

1277



1278

1279 **Figure 6: Consequences of resistance.** a, Unexposed biofilm-adapted lineages were
 1280 tested for resistance over time with no changes observed in their resistance score (additive value of

1281 *all MICs determined for a strain). b, Although the strains adapted to forming better biofilms over*
1282 *time, their resistance score did not change. c, Biofilm viability was tested on 72-hour-biofilms grown*
1283 *on coverslips after treatment with increasing amounts of ciprofloxacin (0, 0.03, 0.3, 3 µg/mL). The*
1284 *strains tested were: cip-plank-L-S1 (resistant but low-biofilm former), control-L-S1 (not resistant but*
1285 *good biofilm former) and cip-biofilm-L-B-S3 (resistant and good biofilm former). Only biofilms*
1286 *produced by cip-biofilm-L-B-S3 were significantly harder to kill with ciprofloxacin. d, 72-hour-biofilms*
1287 *grown on coverslips were pre-treated with 3 µg/mL ciprofloxacin for 90 minutes, they were stained*
1288 *with live/dead stain and fluorescence microscopy was performed in a Zeiss Axio Imager M2. Different*
1289 *strains formed biofilms of variable density. An increased number of live cells was only observed in*
1290 *biofilms produced by the cip-biofilm-L-B-S3 strain, with surviving cells forming dense clusters on the*
1291 *coverslip. e, Pathogenicity (bars) was tested in the Galleria mellonella infection model. Each point*
1292 *indicates the average number of survivors from independent experiments and the bars show the*
1293 *average of these. The strains tested exhibited resistant phenotypes, with diverse biofilm abilities. WT*
1294 *and the unexposed control-L-S1 strain were used as a reference to the assay. Biofilm formation (lines)*
1295 *was measured by the CV assay and on CR plates. Survival was directly correlated with biofilm*
1296 *formation, with the weak biofilm formers causing more deaths in this model. f, Stability of resistance*
1297 *was measured by calculating the average of fold change in MIC per antibiotic, after ten 24-hour*
1298 *passages without any stressor present. For most antibiotics, resistance was stable throughout the*
1299 *accelerated evolution experiment except for cefotaxime. g, Biofilm formation increased significantly*
1300 *for the majority of the tested strains, by the end of the experiment. h, Individual example of an*
1301 *azithromycin resistant strain, which adapted and formed better biofilm over time without losing*
1302 *resistance to azithromycin. Pink line shows the changes in azithromycin MIC over time (line graph,*
1303 *left axis). Bars (bar chart, right axis) show the average biofilm formation from three replicates. Error*
1304 *bars indicate standard deviation i, Individual example of a cefotaxime resistant strain, which*
1305 *adapted to forming better biofilm but lost the resistance to cefotaxime. Purple line shows the*
1306 *changes in cefotaxime MIC over time (line graph, left axis). Bars and error bars are as above.*

1307 **Tables**

1308 **Table 1. Bacterial strains and vectors**

1309

<i>Constructs/ Vectors</i>	Source/ Reference	Description
pDOC-K	(60)	Gene doctoring deletion backbone
pACBSCE	(60)	Gene doctoring helper plasmid
pDOC-K/ <i>acrB</i>	Webber group	<i>acrB</i> deletion construct
pDOC-K/ <i>ramR</i>	Webber group	<i>ramR</i> deletion construct
pDOC-K/ <i>yjcC</i>	Webber group	<i>yjcC</i> deletion construct
pDOC-K/ <i>envZ</i>	Webber group	<i>envZ</i> deletion construct
pDOC-K/ <i>glms</i>	Webber group	Gene doctoring complementation backbone

pDOC-K/ <i>glms/ ramR</i>	Webber group	<i>ramR</i> complementation construct, under native promoter
pDOC-K/ <i>glms/ ramR</i> T18P	Webber group	<i>ramR</i> T18P complementation construct, under native promoter
pDOC-K/ <i>glms/ envZ</i>	Webber group	<i>envZ</i> complementation construct, under constitutive plac promoter
pDOC-K/ <i>glms/ envZ</i> R397H	Webber group	<i>envZ</i> R397H complementation construct, under constitutive plac promoter
pWKS30/ <i>acrB</i>	(61)	<i>acrB</i> complementation construct, under arabinose-inducible pbad promoter
pWKS30/ <i>acrB</i> Q176K	Webber group	<i>acrB</i> -Q176K complementation construct, under arabinose-inducible pbad promoter
pWKS30/ <i>acrB</i> R717L	Webber group	<i>acrB</i> -R717L complementation construct, under arabinose-inducible pbad promoter

Strains	Source/ Reference	Description
<i>Salmonella enterica</i> serovar Typhimurium (14028S)	(62)	Wild type strain
14028S/ Δ <i>acrB</i>	Webber group	<i>acrB</i> deletion strain
14028S/ Δ <i>ramR</i>	Webber group	<i>ramR</i> deletion strain
14028S/ Δ <i>envZ</i>	Webber group	<i>envZ</i> deletion strain
14028S/ Δ <i>acrB</i> / <i>pacrB</i>	Webber group	<i>acrB</i> complementation strain
14028S/ Δ <i>acrB</i> / <i>pacrB</i> R717L	Webber group	<i>acrB</i> R717L complementation strain
14028S/ Δ <i>ramR</i> / <i>pramR</i>	Webber group	<i>ramR</i> complementation strain
14028S/ Δ <i>ramR</i> / <i>pramR</i> T18P	Webber group	<i>ramR</i> T18P complementation strain
14028S/ Δ <i>envZ</i> / <i>penvZ</i>	Webber group	<i>envZ</i> complementation strain

14028S/ $\Delta envZ$ / <i>penvZ</i> R397H	Webber group	<i>envZ</i> R397H complementation strain
14028S/ $\Delta acrB$ / $\Delta ramR$	Webber group	Double deletion strain
14028S/ $\Delta acrB$ / $\Delta ramR$ / <i>pacrB</i>	Webber group	Double deletion strain/ <i>acrB</i> complementation
14028S/ $\Delta acrB$ / $\Delta ramR$ / <i>pacrB</i> (R717L)	Webber group	Double deletion strain/ <i>acrB</i> complementation-SNP variation

1310

1311 **Table 2. Primers used in this study**

Name	Sequence	Use
<i>AcrB</i> -part1 for (EcoRI)	TACGTGAATTCCACGCGGCGATGCCACGGTG	<i>acrB</i> deletion
<i>AcrB</i> -part1 Rev (BamHI)	GCATAGGATCCAAATATAGGGCGATCGATAA	<i>acrB</i> deletion
<i>AcrB</i> -part2 for (XhoI)	TACGTCTCGAGATTGAGCATAGTCATTTCGAC	<i>acrB</i> deletion

<i>AcrB</i> -part2 Rev (NheI)	GCATAGCTAGCGTTTGTGTAATCATTGGGTT	<i>acrB</i> deletion
<i>RamR</i> part1-For (EcoRI)	TACGTGAATTCAAACTCGTCAGCGGCTCCCG	<i>ramR</i> deletion
<i>RamR</i> -part1 Rev (BamHI)	GCATAGGATCCTTTTTTGTCTTCACTCTTCG	<i>ramR</i> deletion
<i>RamR</i> -part2 for (XhoI)	TACGTCTCGAGTGGCGCGCGCTGACTCGCGA	<i>ramR</i> deletion
<i>RamR</i> -part2 Rev (NheI)	GCATAGCTAGCTATCCTCGCCCGCATAGACT	<i>ramR</i> deletion
<i>EnvZ</i> _part1_For (EcoRI)	TACGTGAATTCCGCGAGATGTTC	<i>envZ</i> deletion
<i>EnvZ</i> _part1_Rev (BamHI)	GGATCCGGATCCAACTTCGC	<i>envZ</i> deletion
<i>EnvZ</i> _part2_For (XhoI)	TACGTCTCGAGCGCGTCCAG	<i>envZ</i> deletion

<i>EnvZ</i> _part2_Rev	AGTACTAGTGCTGTTCGATCTGGCGATCCCGAC	<i>envZ</i> deletion
(SpeI)		
<i>Glms</i> _part1_For	TACGTGAATTCGCTCGAAGGCGCGCTGAAG	pDOC-K/ <i>glms</i>
(EcoRI)		generation
<i>Glms</i> _part1_Rev	ACGTAGGTACCCGGCCTTCTGCCTGGTACTACATTTG	pDOC-K/ <i>glms</i>
(KpnI)		generation
<i>Glms</i> _part2_for	TACGTCTCGAGCATATGCCCGGGGCGGCCGCAAGCTTTCGACAGACGGCCTTTTT	pDOC-K/ <i>glms</i>
(XhoI)-MCS	TTG	generation
<i>Glms</i> _part2_Rev	GCATAGCTAGCCGGTCAATTTCCCCATTCCC	pDOC-K/ <i>glms</i>
(NheI)		generation
<i>RamR</i> -compl-For	GCATACTCGAGTTCATGCGGCAGCCCTTG	<i>ramR</i>
(XhoI)		complementation
<i>RamR</i> -compl-Rev	ACGTAAAGCTTTTATTGCTCCTCGCGAGTCAGC	<i>ramR</i>
(HindIII)		complementation

<i>EnvZ</i> -compl-For (XhoI)	ATCACTCTCGAGTTTACACTTTATGCTTCCGGCTCGTATGTTGCAGACCGTCTGGG GCCTGG	<i>envZ</i> complementation
<i>EnvZ</i> -compl-Rev (HindIII)	GGACGTAAGCTTTTATGCCTCTTTTGTTCGTCCCCTGGAC	<i>envZ</i> complementation
<i>GyrB</i> -RT-For	GGAAGGGGACTCCGCGGGCG	q-RT PCR
<i>GyrB</i> -RT-Rev	CAGCGGCGGCTGCGCAATGT	q-RT PCR
<i>RamA</i> -RT-For	CGCTCAGGTTATCGACACGA	q-RT PCR
<i>RamA</i> -RT-Rev	CCACTTGGGAATACCCCGCAT	q-RT PCR
<i>OmpF</i> -RT-For	GGCGGCGCCTATACTGATAA	q-RT PCR
<i>OmpF</i> -RT-Rev	CGAAAGAGAGACCGTCCACC	q-RT PCR
<i>OmpC</i> -RT-For	TTATGCAATCGGCGAAGGCT	q-RT PCR
<i>OmpC</i> -RT-Rev	GTTACCATACAGGCGAGCGT	q-RT PCR
<i>CsgA</i> -RT-For	CATCGACCAGTGGAACGCTA	q-RT PCR
<i>CsgA</i> -RT-Rev	TACGCTGGAATCAGATGCGG	q-RT PCR
<i>CsgB</i> -RT-For	TGCAACCGCGACAAATTATGA	q-RT PCR

CsgB-RT-Rev

TTGACCAATAATGGCCGCCT

q-RT PCR

1312